To my family

A BACTERIAL LIVING THERAPEUTICS WITH ENGINEERED PROTEIN SECRETION CIRCUITS TO ELIMINATE BREAST CANCER CELLS

A THESIS SUBMITTED TO
THE GRADUATE SCHOOL OF ENGINEERING AND SCIENCE
OF BILKENT UNIVERSITY
IN PARTIAL FULFILLMENT OF THE REQUIREMENT FOR
THE DEGREE OF
MASTER OF SCIENCE
IN
MATERIALS SCIENCE AND NANOTECHNOLOGY

BY

GOZEEL BINTE SHAHID

JANUARY 2024

A BACTERIAL LIVING THERAPEUTICS WITH ENGINEERED PROTEIN SECRETION CIRCUITS TO ELIMINATE BREAST CANCER CELLS

By Gozeel Binte Shahid

January 2024

We certify that we have read this dissertation and that in our opinion it is fully adequate, in scope and in quality, as a thesis for the degree of Master of Science.

_____
Urartu Özgür Şafak Şeker (Advisor)

_____
Işık G. Yuluğ

_____
Yüksel Ürün

Approved for the Graduate School of Engineering and Science:

_____

Orhan Arıkan
Director of the Graduate School

ABSTRACT

A BACTERIAL LIVING THERAPEUTICS WITH ENGINEERED PROTEIN SECRETION CIRCUITS TO ELIMINATE BREAST CANCER CELLS

Gozeel Binte Shahid

M.Sc in Materials Science and Nanotechnology

Advisor: Urartu Özgür Şafak Şeker

January, 2024

Cancer therapy often faces limitations due to potential side effects, prompting scientific interest in bacteria-based living cancer treatments. Yet, the complete utilization of bacteria in therapeutic applications confronts engineering hurdles. This thesis focuses on introducing a novel bacterial mechanism specifically intended to target and eliminate breast cancer cells. Our innovative approach involves modifying *Escherichia coli (E. coli)* to secrete a Shiga toxin called HlyE, a pore-forming protein that binds to HER2 receptors found on breast cancer cells. This binding process is facilitated by a nanobody expressed on the bacterial surface through the Ag43 autotransporter protein system. Our research demonstrates the effective binding of the nanobody to HER2+ cells in laboratory conditions (*in vitro*). Utilizing the YebF secretion system, we successfully leverage the secretion of HlyE, leading to the eradication of the targeted cancer cells. These outcomes emphasize the significant potential of our engineered bacteria as an innovative and promising strategy for breast cancer treatment. This

pioneering approach represents a groundbreaking development in the field of cancer therapeutics. By harnessing the unique properties of bacteria and utilizing advanced engineering techniques, we've succeeded in creating a targeted and potent system capable of attacking breast cancer cells specifically marked by the HER2 receptor. Our study lays a robust foundation for future exploration and development in the realm of bacterial-based cancer therapies, offering potential solutions to the challenges encountered in traditional cancer treatment methods.

Keywords: Living Therapeutics, Cancer Therapeutics, Synthetic Biology

ÖZET

MEME KANSERİ HÜCRELERİNİ ORTADAN KALDIRMAK İÇİN TASARLANMIŞ PROTEİN SALGILAMA DEVRELERİ SAHİP YAŞAYAN BAKTERİYEL TERAPÖTİK

Gozeel Binte Shahid

Malzeme Bilimi ve Nanoteknoloji, Yüksek Lisans

Tez Danışmanı: Urartu Özgür Şafak Şeker

Ocak, 2024

Kanser tedavisi genellikle potansiyel yan etkiler nedeniyle sınırlamalarla karşılaşır, bu da bilim dünyasını bakteri tabanlı canlı kanser tedavilerine yönlendirir. Ancak, bakterilerin terapötik uygulamalarda tam olarak kullanımı, bir takım zorluklar ile karşılaşır. Bu tez, özellikle meme kanseri hücrelerini hedef alıp ortadan kaldırmak üzere tasarlanmış yeni bir bakteriyel mekanizmayı tanıtmaya odaklanmaktadır. Yenilikçi yaklaşımımız, Escherichia coli (E. coli) bakterisini, meme kanseri hücrelerinde bulunan HER2 reseptörlerine bağlanan bir Shiga toksini olan HlyE'yi salgılamak üzere değiştirmeyi içerir. Bu bağlanma süreci, Ag43 ototransporter protein sistemi aracılığıyla bakteri yüzeyinde ifade edilen bir nanobody tarafından gerçekleştirilir. Araştırmamız, nanobody

molekülünün laboratuvar koşullarında HER2+ hücrelere etkin bir şekilde bağlandığını (in vitro) göstermektedir. Kanser hücrelerinin ortadan kaldırılmasını hedefleyen HlyE'nin salgılanmasını, YebF salgı sistemini kullanarak başarıyla sağlıyoruz. Bu sonuçlar, geliştirdiğimiz bakterilerin, meme kanseri tedavisi için yenilikçi ve umut verici bir strateji olarak önemli potansiyelini vurgular. Bu öncü yaklaşım, kanser terapisi alanında çığır açan bir gelişmeyi temsil eder. Bakterilerin benzersiz özelliklerini kullanarak ve gelişmiş mühendislik tekniklerini uygulayarak, HER2 reseptörü tarafından belirlenen özellikle meme kanseri hücrelerini hedefleyen bir sistem yaratmayı başardık. Çalışmamız, bakteri tabanlı kanser tedavilerinde karşılaşılan geleneksel tedavi yöntemlerindeki zorluklara potansiyel çözümler sunarak, gelecekteki keşif ve geliştirmeler için sağlam bir temel oluşturmaktadır.

Anahtar Kelimeler: Yaşayan İlaçlar, Kanser Terapötik, Sentetik Biyoloji

ACKNOWLEDGEMENTS

Embarking on a three-year odyssey to craft this master's thesis has been a journey marked by challenges and excitement. The privilege of working within the esteemed confines of UNAM, one of Turkey's premier research organizations, has been both an honor and a crucible for growth.

Foremost, I extend my deepest gratitude to my advisor, Asst. Prof. Urartu Özgür Şafak Şeker. His unwavering guidance and mentorship have not only rendered this project possible but have also catalyzed my evolution as a scientist. I am profoundly thankful for his acceptance into his lab, his persistent encouragement, and most importantly, for believing in my potential.

A heartfelt acknowledgment is due to the invaluable members of the Synthetic Biosystems Lab, both past and present. Special mention goes to Dr. Recep Erdem Ahan, whose guidance and friendship have been instrumental in shaping the trajectory of this project. I am also indebted to Julian Ostaku, whose initiation of this project and year-long training laid the foundations crucial for my assimilation into the lab.

A chorus of appreciation extends to the entire lab team, including Dr. Ebru Şahin Kehribar, Dr. Elif Duman, Dr. Burcu Ergun, Dr. Recep Erdem Ahan, Suat Tüçer, Merve Erden, Cemile Elif Özçelik, Senem Şen, Mehmet Emin Bakar (special thanks to Mehmet for assisting me with protein purification), Doğuş Akboğa, Aslı Semerci, Melis Karaca, Cem Dirse Polat, Ahmet Hınçer, Nazlıcan Tunç, Abdurahman Atilla, Merve Canpulat, Merve Yavuz, Ece Avcı, Derin Akman, Aslı Doğruer, Damla Albayrak, and Fayiti Fuerkaiti, Each of them has left an

indelible mark on this academic endeavor.

In the realm of personal support, my heartfelt thanks go to Ghada Ibrahim for her unwavering belief in me and for her being by my side through tough times. I'd like to thank Maryam Jamil, whose lojman became my sanctum for compiling most of this thesis. Her friendship in my last semester has been pivotal. I hold immense appreciation for Kazi Haisam Siddiqui for his steadfast encouragement and cherished friendship, even across miles. Gratitude envelops my family—my mother Saboohi Shahid, my sister Awayah Shahid, and my brother Muhammad Bin Shahid—for being pillars of strength, sanity, and unwavering support. Special mention to my furry confidant, Sheiru, whose cuddles and cuteness provided solace during challenging times.

A poignant tribute is reserved for my baba Shahid Sattar Awan (in heaven). My everyday efforts and accomplishments are an echo of your influence, and I miss you profoundly, especially in moments of triumph like this.

This project was partially funded by TÜBITAK Project no 123M168.

This thesis stands as a testament not only to academic rigor but to the profound network of support and encouragement that has shaped its narrative. Each person mentioned has played a unique role, and for that, I am eternally grateful.

TABLE OF CONTENTS

LIST OF TABLES

LIST OF FIGURES

CHAPTER I: INTRODUCTION

1.1 Emerging Trends in Cancer Research

Cancer, a complex and multifaceted class of diseases characterized by uncontrolled cell proliferation and genomic instability, remains a prominent challenge in contemporary medical research. The relentless pursuit of innovative strategies for its treatment and management has led to remarkable progress in the field. Recent years have witnessed a profound transformation in cancer research, driven by advances in various domains. Epigenetics, a frontier discipline, has unveiled the intricate molecular mechanisms governing gene expression and chromatin modifications, offering profound insights into the etiology of cancer and potential therapeutic targets[1]. Immunotherapy, particularly immune checkpoint inhibitors, has revolutionized cancer treatment by leveraging the immune system's intrinsic capabilities to identify and eliminate malignant cells[2, 3]. Moreover, nano-based pharmaceuticals[4] and nanotechnology have redefined drug delivery strategies, enhancing targeted drug delivery and minimizing off-target effects[5]. These nanocarriers exhibit exceptional potential in addressing the formidable challenge of drug resistance and improving the therapeutic index of anti-cancer agents. Furthermore, the exploration of plant-derived bioactive compounds has gained momentum, with phytochemicals demonstrating significant anti-cancer properties[6], often through novel mechanisms of action. mRNA vaccines, most notably exemplified by the COVID-19 pandemic, have spurred interest in personalized mRNA-based cancer vaccines, which hold great promise for eliciting specific anti-tumor immune responses[7,8]. Smart stimuli-responsive implantable drug delivery systems[9]

are a promising avenue in precision medicine, enabling real-time drug release modulation and dose adjustments according to the patient's evolving condition.

Towards the convergence of advanced biotechnologies, synthetic biology is emerging as a transformative approach for cancer therapy. Living therapeutics to treat cancer is a novel domain possible through the aid of synthetic biology. Bacteria-based cancer therapeutics, a subset of synthetic biology, leverages genetically engineered bacteria to selectively target and destroy cancer cells within the tumor microenvironment[10]. These live therapeutics exhibit remarkable potential in eradicating tumor heterogeneity and have the capacity to deliver multiple therapeutic payloads, a feat hitherto unattainable[10–13]. Synthetic biology empowers the rational design and customization of these bacterial agents, ensuring precise and adaptive tumor targeting, while also mitigating potential safety concerns.

1.2 Synthetic Biology’s Impact on Precision Cancer Therapies

The advent of synthetic biology within the realm of precision cancer therapies has unleashed a wave of transformative potential, revolutionizing the landscape of cancer treatment strategies. By applying engineering principles to modify living cells, synthetic biology offers a highly adaptable and programmable platform for the development of innovative therapeutic approaches. This platform enables the creation of artificial gene circuits that function as molecular decision-making devices, thereby empowering "sense-and-respond" adaptive therapies, which are characterized by the ability to dynamically adjust their behavior in response to changing disease conditions[14].

The quest for precision in cancer therapy is paramount, aiming to maximize the specificity of treatment while minimizing collateral damage to healthy tissues. Synthetic biology provides a powerful arsenal of tools and techniques to address this challenge. Gene circuits designed within the framework of synthetic biology can effectively discriminate between malignant and healthy cells, executing therapeutic actions selectively[14,15]. This level of precision is unprecedented in the field of cancer therapy, offering the potential to mitigate the side effects and limitations associated with conventional treatments.

The core components of synthetic biology-based gene circuits include sensors that detect user-defined inputs, processors that make decisions based on these inputs, and actuators that generate the desired therapeutic response. Furthermore, synthetic biology circuits can incorporate a variety of regulatory mechanisms, such as transcriptional or post-transcriptional control, including microRNAs and protein-based signaling cascades. Additionally, endogenous inputs, such as transcripts or proteins that distinguish between cell types, enable these gene circuits to sense and respond to the intricacies of the tumor microenvironment[15].

There are profound implications of synthetic biology in the realm of precision cancer therapies, which allows intricate design and application of live therapeutics, including bacteria-based therapeutic systems. The potential of these synthetic biology-driven living therapeutic approaches to transform the landscape of cancer treatment, optimizing therapeutic precision, and minimizing adverse effects, represents a promising avenue for future clinical applications.

1.3 Living Therapeutics and Synthetic Biology

The concept of living therapeutics, a quintessential manifestation of synthetic biology, has its roots in the late 19th century. Early pioneers, such as Dr. Busch and Dr. Coley, made groundbreaking observations and interventions that laid the foundation for contemporary developments in the field. In 1867, Dr. Busch, a medical physician, made a striking observation when one of his cancer patients went into remission after contracting a *Streptococcus pyogenes* infection. This serendipitous event marked the first hint at the therapeutic potential of living microorganisms[17]. Two decades later, Dr. William Coley directly injected *Streptococcus* bacteria into a tumor site to incite an immune response capable of eradicating cancer cells[18]. This groundbreaking strategy extended his patient's life by eight years. However, challenges emerged as some patients suffered from complications due to the infection. To address these issues, Coley modified his approach, opting for the injection of a mixture of heat-killed bacteria, later known as "Coley's Toxins." This shift toward a safer and more controlled intervention method marked a significant advancement in the use of microorganisms for therapeutic purposes.

In contemporary times, living therapeutics represent a new frontier in healthcare, building on the insights derived from the work of Busch and Coley[19]. These modern interventions rely on engineered microbial organisms that possess integrated sensing mechanisms. These mechanisms allow the organisms to respond to a wide array of cues, including biomarkers, temperature, chemicals, hypoxia, pH, and other microenvironmental factors. Furthermore, these engineered organisms incorporate sophisticated genetic toolkits, enabling them

to release therapeutics on-site[12].

Living therapeutics, a product of the convergence between synthetic biology and medicine, hold immense promise for revolutionizing disease treatment. These innovative interventions promise targeted, precise, and highly effective therapeutic strategies for addressing complex and challenging medical conditions, ushering in a new era of healthcare where personalization and adaptability are at the forefront. As synthetic biology continues to advance, living therapeutics are poised to play a pivotal role in shaping the future of medical treatment.

1.4 Bacteria-based Living Therapeutics for Cancer

Recent advancements in scientific research have ignited a growing fascination with the therapeutic potential of bacteria, ushering in a transformative shift in disease management strategies[10]. A more profound comprehension of the intricate interplay between bacteria and human physiology has propelled the domain of bacteria-based therapeutics, offering novel prospects for innovative treatments. Traditionally, bacteria were predominantly studied for their pathogenic attributes. Nevertheless, recent strides in biology and synthetic biology methodologies have unveiled their latent therapeutic applications. The versatility of bacteria empowers researchers to harness their capabilities in diverse ways, encompassing the production and targeted delivery of therapeutic agents to specific tissues. This bacterial approach bestows significant advantages over conventional drug therapies, enabling precise targeting of diseased tissues and cost-effective mass production[11].

Traditional cancer treatments, typified by chemotherapy and radiation therapy, frequently entail an array of undesired side effects, including harm to healthy tissue and a lack of specificity[20]. Bacteria, with their innate capacity to selectively inhabit and proliferate within specific tissues[21], hold the potential to surmount this challenge by offering a new paradigm [10,11,12,13,21,22,23]. Engineered bacterial vectors devised for the direct delivery of cancer-eradicating agents to the cancer site promise more pinpointed and efficacious treatment, thereby diminishing the risk of side effects. Furthermore, certain bacteria have exhibited the ability to produce compounds with direct cancer cell-killing properties or to stimulate the body's immune system to combat the cancer[23]. The nexus between cancer and bacterial immunotherapy, as aforementioned, traces its roots to the 19th-century experiments conducted by Coley, which established that specific bacterial infections could induce cancer remission by provoking an immune response. Nonetheless, despite this historical backdrop, the utilization of bacteria as therapeutic agents remains an underexplored frontier and has not achieved the widespread adoption seen in traditional drug therapies. This can be attributed, in part, to the complexities involved in bacterial engineering. However, given the headway in synthetic biology, these challenges can be surmounted. The precision afforded by synthetic biology in manipulating and governing the genetic makeup of bacteria has unveiled novel avenues for tailored anti-cancer therapeutic strategies with enhanced specificity and efficacy[13,25,26,27].

Thus far, synthetic biology has empowered researchers to manipulate bacteria to target tumor cells with enhanced precision[28]. By modifying bacteria to express specific molecules, they can be programmed to adhere to tumor cells[11] and

introduce payloads such as macromolecules into these cells. Augmenting the delivery efficiency through the integration of certain genes can enhance the replication of bacteria within the cells[29]. Additionally, bacteria have been engineered to deliver drugs by either creating pores in cell membranes or lysing the cells, thereby releasing drugs within tumor cells[30]. Some bacteria have been designed to metabolize waste produced by tumors[23], while others have been equipped with a quorum-sensing system to trigger drug release[12]. Genetic circuits within bacteria have also been developed to function as controlled delivery systems, releasing cargo to tumor cells[13]. Further refinement of these genetic circuits has been explored, exemplified by the expression of the invasin gene, which has demonstrated an increased capacity to facilitate bacterial uptake into phagosomes and enhance the invasion efficiency of otherwise extracellular bacteria[31]. Notwithstanding the progress in developing bacterial therapies, a major challenge lies in the absence of *in vitro* tools for evaluating the behavior of bacteria within a tumor-like environment. However, recent breakthroughs have enabled high-throughput and long-term cultivation of bacteria within the core of tumor spheroids *in vitro*[32].

1.5 Engineering Gene Circuits in Bacteria with Synthetic Biology

In recent years, the field of synthetic biology has witnessed significant advancements in the engineering of gene circuits within bacterial hosts[33,34]. This cutting-edge approach entails the application of genetic manipulation and molecular biology techniques to meticulously design, construct, and regulate intricate networks of genes within bacterial organisms. The primary objective is to confer specific functionalities upon these bacteria, such as their ability to

respond to environmental cues[35] or facilitate the production of valuable compounds[36], achieved through the precise regulation of gene expression. These circuits, commonly referred to as genetic circuits or gene networks, consist of interconnected genetic elements, including promoters, repressors, and various regulatory sequences. This architecture provides researchers with the capability to program bacteria for a wide range of tasks, spanning from biosensing and bio-actuation to the synthesis of therapeutic proteins[37–39].

An illustrative example of such engineering endeavors is the creation of gene circuits in *Escherichia coli* (*E. coli*), a frequently utilized bacterial host. These circuits can be purposefully designed to respond to specific inputs, such as environmental signals or molecular triggers, and yield desired outputs, including the synthesis of therapeutic agents or the activation of specific metabolic pathways[40,41].

The process of engineering gene circuits in bacteria entails precise placement of genetic components, fine-tuning of promoter strengths, and optimization of regulatory elements. Leveraging tools from synthetic biology, such as CRISPR-Cas systems[42], plasmid construction, and gene synthesis techniques, plays an instrumental role in the realization of these objectives.

Engineered gene circuits hold immense promise across various domains, including biotechnology, medical research, and environmental science. They can be harnessed to advance novel therapeutic strategies, drive innovation in biofuel production, and contribute to the development of biosensors for environmental pollutant detection[43–45].

As research in the field of synthetic biology continues to advance, the capacity to engineer gene circuits in bacterial hosts opens new avenues for scientific innovation, thereby fostering the progress of knowledge and the emergence of practical applications with profound societal implications.

1.6 Aim of the Study

This work is partially described in the following publication[46]:

Gozeel Binte Shahid[1], Recep Erdem Ahan[1], Julian Ostaku[1], Urartu Ozgur Safak Seker[1,*]

[1]UNAM- Institute of Materials Science and Nanotechnology, National Nanotechnology Research Center, Bilkent University, Ankara 06800, Turkey.

[*]Corresponding author : urartu@bilkent.edu.tr

G. B. Shahid, R. E. Ahan, J. Ostaku, and U. O. S. Seker, "A Bacterial Living Therapeutics with Engineered Protein Secretion Circuits To Eliminate Breast Cancer Cells." *bioRxiv*, p. 2023.04.27.538589, Apr. 27, 2023. doi: 10.1101/2023.04.27.538589.

In this thesis, we introduce a bacterial design that addresses two primary challenges in cancer therapy: the attachment to target cells and effective delivery of therapeutic agents. We modified the bacterial strain *E. coli BL21* to secrete a toxin and adhere to HER2 receptors on breast cancer cells. This attachment is

facilitated by the expression of a nanobody known as 2Rs15d on the bacteria's surface through the Ag43 autotransporter protein system[32,33]. This anti-HER2 nanobody has previously demonstrated its ability to efficiently bind to HER2+ cells both in laboratory and animal studies[49]. To secrete the pore-forming toxin HlyE, we utilized the YebF secretion system, a type VI secretion system known for its versatility in secreting various compounds, including proteins, toxins, and other molecules[50]. A simple diagrammatic illustration is given in Figure 1.

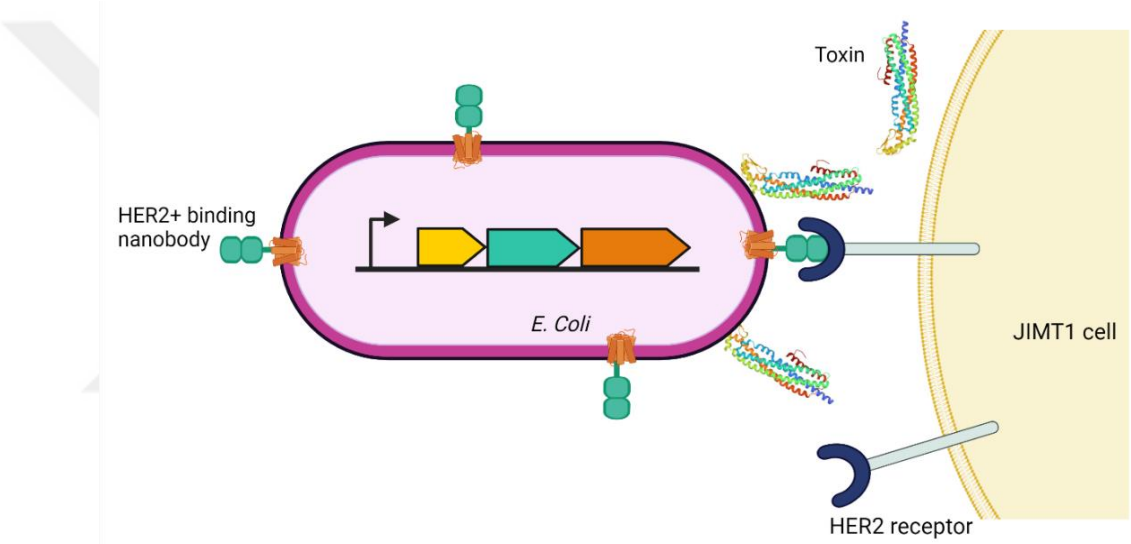

Figure 1: The Aim of this thesis. *E. coli BL21* is engineered with surface-displayed nanobody to bind to HER2 receptors on JIMT1 cells, imparting specificity to the proposed system. Pore-forming toxin HlyE is secreted from *E. coli* to subsequently eliminate the cancer cell.

To evaluate the effectiveness of our proposed bacterial design, we conducted experiments on JIMT1 HER2+ cells. To enhance the accuracy of our findings, we used cell spheroids, which offer several advantages, such as the ability to replicate the complex conditions found in tumor microenvironment, improved cell-to-cell interactions, and enhanced cell viability. Our experiments

demonstrated that the engineered bacteria are indeed functional and displayed promising results in both 2D and 3D cell culture assays. These findings highlight the potential of our approach for using engineered bacteria as an innovative strategy for treating breast cancer. We are optimistic that further investigations, including *in vivo* studies, will provide deeper insights into the possibilities offered by this approach.

CHAPTER II: MATERIALS AND METHODS

2.1 Bacterial Cell Strains, Growth Conditions, Maintenance and Transformation

The experiments for cloning utilized *E. coli* DH5α PRO cells. These cells were grown in Luria-Bertani (LB) medium, which consists of 8 g/l tryptone, 8 g/l NaCl, and 4 g/l yeast extract, with their corresponding antibiotics at 37 °C and 200 rpm. Overnight cultures were prepared from cell stocks incubated in the same medium for 16 hours under the same conditions. The transformed bacteria cell stocks were stored at -80°C in 1 ml aliquots, conserved using a 25% glycerol solution combined with Lysogeny Broth (LB). For protein expression and purification, *E. coli BL21* (DE3) strain was used.

Unless specifically mentioned, plasmids are introduced into bacterial cells through a chemical transformation process. To create chemically competent cells, the cells were initially inoculated in fresh LB along with suitable antibiotics from the -80°C cell stock and left to grow overnight. The following day, these cells were re-inoculated in fresh LB with a 1:100 dilution. When the OD600 reached between 0.3 - 0.5, the cells were cooled on ice for 10 minutes. After cooling, the cells were gathered via centrifugation at 1000xg for 10 minutes at 4°C. The resulting cell pellet was suspended in TSS Buffer at a 1:10 volume ratio of the initial growth and divided into 100µl aliquots per microcentrifuge tube, subsequently stored at -80°C.

For the transformation process, the aliquoted cell stock was thawed on ice for 30 minutes. In this transformation phase, 100 ng of intact plasmid, whole Gibson

assembly reaction, or entire T4 ligation reaction was added to the thawed cells and left to incubate on ice for 20 minutes. The cells underwent a heat shock at 42°C for 45 seconds. After the heat shock, the cells were placed back on ice for 2 minutes. Following this, 250µl of LB was introduced to the cells, and the mixture was incubated at 37°C for 45 minutes in a shaking incubator set at 200rpm. Once the incubation period was completed, the cells were centrifuged, discarding 250µl of the supernatant. The resulting cell pellet was resuspended with the remaining supernatant, and these resuspended cells were spread onto LB-agar containing the appropriate antibiotics.

2.2 Plasmid Construction and Cloning

To construct the pET22b(+) T7-LacO PelB 2Rs15d Ag43 plasmid, a pET22b Ag43 160N 6h sfGFP AmpR plasmid was used as the template[47]. The nanobody gene was amplified through Polymerase Chain Reaction (PCR) from the ordered gene fragment, followed by restriction digestion of the pET22b Ag43 160N sfGFP AmpR to obtain the backbone. The 2Rs15d nanobody was cloned downstream of the T7 LacO promoter using primers JO1 and JO2 (all primer sequences are given in Appendix B). After gel extraction, the parts were assembled through Gibson Assembly (recipe for reaction mix is given in Appendix E), and the final product was transformed into *E. coli* DH5α. Two colonies were selected for sequencing after verification of the correct plasmid. The plasmid was then transferred into *E. coli BL21* (DE3). A histidine tag was added to confirm its expression on the surface of *E. coli BL21* (DE3) through Western Blotting.

To construct pTetO Yebf HlyE 6xHis, the backbone was taken from pZa HlyE

YebF CmR vector, and Hemolysin E was amplified from the same vector. The backbone was amplified using primers pREA29 and pREA78, and Hemolysin E was amplified using JO29 and EK pBAD rev primers and a pZa pL-tetO YebF HlyE 6his CmR vector template. The parts were cloned through Gibson Assembly and chemically transformed into *E. coli* PRO DH5α. Colony PCR was performed to verify the cloning, and two colonies were selected for sequencing after validation. Sequencing results for all cloning experiments can be found in Appendix D.

To construct pZa native TetO Yebf HlyE 6xHis-mScarlet, the mScarlet insert was amplified from an Addgene plasmid using pGB1-pGB2 primers and cloned into the pTetO Yebf HlyE 6xHis backbone. The parts were assembled through Gibson Assembly and transformed into *E. coli* DH5α PRO. The cloning was verified through NGS sequencing. Double transformation was performed to obtain *Bl21* pET22b T7 lacO his 2Rs15d Ag43 AmpR pZa native teto HlyE Yebf his CMR-mScarlet, followed by plasmid isolation and PCR. The mScarlet was also directly transformed into *Bl21* competent cells to obtain *E. coli Bl21*-mScarlet. The sequences the genetic parts used in this study are given in Appendix A. All of the constructs and maps for the cloning experiments are given in appendix C.

2.3 Plasmid Isolation, NGS and Sequence Alignment using Geneious Software

Plasmid isolation was done with miniprep method using the GeneJET Plasmid Miniprep Kit. 3ml bacteria was cultured overnight at 37ºC, and next day it was centrifuged at 8000 rpm 4ºC for 5 minutes. Following this, the protocol given in the kit was followed exactly.

Sequencing was done using Next-Generation Sequencing (NGS). Following plasmid isolation, 20µl was inserted in PCR tube, containing about 1500ng of DNA content. This was sent for NGS sequencing and results were received via email. Around 1000-2000 ng of DNA, was dispensed into PCR tubes. The ensuing NGS results were disseminated via email.

To ensure a comprehensive comparison between the obtained NGS results and the expected plasmid map, the map was retrieved in .gb format from Benchling.com. The Geneious software played a crucial role in facilitating the alignment of the map with a reference. Sequence files from Genewiz company and .gb files exported from Benchling.com for vectors were imported using the 'file>import>from file' option. After choosing this option, a new window appeared to navigate and select the folder containing .abi to import all files. To align the specific sequences, they were brought into the primary working windows. By selecting 'align/assemble>pairwise alignment' from the upper panel, a new window opened allowing the user to define specific alignment parameters. The chosen settings included automatic determination of directions, global alignments with free and gaps, and a 50% similarity threshold to align the sequences.

2.4 SDS-Page and Western Blotting

The samples underwent treatment by heating at 95°C for 5 minutes in the presence of 1x SDS loading buffer, followed by separation through electrophoresis on a 15% SDS-polyacrylamide gel. Subsequently, the gel was stained using a Coomassie blue solution for about 1 hour with continuous agitation, then de-stained in a solution composed of 60% ddH2O, 30% methanol,

and 10% acetic acid until the bands became visible.

For the Western blot analysis, the gel was transferred to a PVDF membrane utilizing a Trans-Blot Turbo apparatus (Bio-Rad). The membrane was then subjected to a 1-hour blocking step at room temperature using 5% milk in TBS-T buffer. Following this, the membrane was exposed to a 1:10,000 dilution of primary anti-His mouse antibodies in 5% milk-TBS-T, incubated overnight at 4°C. Subsequently, the membrane was washed with TBS-T and further incubated for 1 hour at room temperature with a 1:10,000 dilution of HRP-conjugated goat anti-mouse secondary antibodies (Abcam ab6789-1 MG) in 5% milk-TBS-T. After multiple TBS-T washes, the membrane was treated with ECL substrates (Bio-Rad 170-5060) and visualized utilizing a Vilber Fusion Solo S system.

For the Western blot analysis of supernatant samples, trichloroacetic acid (TCA) precipitation was used for sample preparation. Initially, cells were lysed in a buffer (50 mM Tris-HCl pH 7.5, 150 mM NaCl, 1% Triton X-100, 0.1% SDS, and 1 mM PMSF) for 30 minutes on ice. The lysates were centrifuged at 14,000 g for 15 minutes at 4°C to eliminate insoluble debris. The resulting supernatants were mixed with 10% TCA and left to incubate at 4°C for 1 hour. Subsequently, the samples were centrifuged at 14,000 g for 15 minutes at 4°C to form a pellet of precipitated proteins. The pellet underwent two washes with ice-cold acetone and was air-dried. This dried pellet was then reconstituted in loading buffer (0.125 M Tris-HCl pH 6.8, 4% SDS, 20% glycerol, and 0.2% bromophenol blue), and heated at 95°C for 5 minutes to denature the proteins. The treated samples were then subjected to SDS-PAGE and transferred to a PVDF membrane for subsequent Western blot analysis.

2.5 Immunocytochemistry (ICC)

The antibodies were diluted to a ratio of 1:300 in a buffer comprising 1% BSA in PBST (PBS with 0.1% Tween 20). Following an overnight incubation under inducing conditions, a cell culture volume of 5-10 mL was centrifuged at 4000 g for 15 minutes. The resulting cell pellet was treated with 1 mL of 4% formaldehyde diluted in PBS and left to incubate at room temperature for 30 minutes.

For the washing procedure, the cells were centrifuged at 1500 g for 5 minutes and subsequently resuspended in 1 mL of PBS, repeated twice. To prevent non-specific binding of antibodies, slides were exposed to a blocking solution containing 1% BSA in PBST for 30 minutes. After the blocking solution was removed, cells were exposed to the primary antibody for a 2-hour duration at room temperature. Following a wash in 500 μL of 1X PBS, the cells were incubated with a secondary antibody at a dilution of 1:500 overnight in a dark environment at +4 ºC. The cells were washed twice in PBS and allowed to air-dry. To protect the staining, a drop of mounting medium was added, and a cover glass was affixed to each slide using nail polish. Subsequently, the slides were examined under a fluorescence microscope.

2.6 Protein Purification using FPLC

The purification process for the HlyE protein involved several steps. Initially, HisTrap column purification was carried out using FPLC (Fast Protein Liquid Chromatography). The *E. Coli* strain pZa pL-tetO YebF HlyE his AmpR was cultured and induced overnight with IPTG at 16ºC. Upon centrifugation at 8000g for 5 minutes, the resulting pellet was resuspended in binding buffer (20mM

Na2HPO4, 500mM NaCl, 20mM imidazole, pH=7.4), with the addition of 1mM PMSF as a protease inhibitor.

The resuspended cells underwent a series of rapid freezing and thawing cycles using liquid nitrogen, followed by sonication (10 cycles at 25% amplitude) to facilitate effective cell lysis and release of the target HlyE protein. The lysate was then subjected to centrifugation at 12000g for 40 minutes, yielding a clarified supernatant that underwent subsequent FPLC purification. The bound protein was eluted using an elution buffer (20mM Na2HPO4, 500mM NaCl, 500mM imidazole, pH=7.4).

To render the protein suitable for use in mammalian cells, the HlyE toxin underwent a buffer exchange with 1xPBS using a HiTrap desalting column, as the initial buffer containing imidazole was deemed toxic to these cells. Following the buffer exchange, the purified HlyE was concentrated into three different concentrations (750 ng/µl, 1200 ng/µl, and 2000 ng/µl), determined via BCA assay.

Subsequently, the purified HlyE protein was tested on JIMT1 mammalian cells, which were seeded in a 96-well plate for experimental analysis.

2.7 Cultivation, Maintenance, Growth and Counting of Mammalian Cells

The HER2+ breast cancer cell line JIMT1, genetically modified with GFP, was supplied by the Molecular Biology and Genetics Department at Bilkent University and stored at a temperature of -80ºC. They were grown in 88% low-

glucose Dulbecco's Modified Eagle Medium (DMEM) combined with 10% Fetal Bovine Serum (FBS), 1% Penicillin/Streptomycin (Pen/Strep) antibiotic, and 1% L-glutamine. When starting a new cell stock, the process commenced by transferring the contents of the thawed stock vial to 13 mL of fresh media, followed by centrifugation at 2500 rpm for 5 minutes. The resulting supernatant was carefully removed, and the pellet was then resuspended in 1 mL of fresh medium. This suspension was added to a T25 flask along with 2 mL of media and kept in an incubator set at 37°C and 5% CO2. Media changes occurred every two days after rinsing with 3mL 1X PBS.

When the cells reached 80%-90% confluence, they underwent passaging, involving a specific procedure. Firstly, a wash with 10 mL PBS was performed, followed by the addition of 3 mL trypsin, and a 5-minute incubation to detach the cells from the flask surface. The contents were then transferred to a 15 mL falcon tube containing 10 mL fresh medium, and centrifuged for 5 minutes at 2500 rpm. The resulting supernatant was discarded, and the pellet was reconstituted in 1 mL fresh media. Cell counting was done by diluting 10 µL of the sample in a PCR tube with fresh media at a 1:10 ratio. Then, 10 µL of this diluted solution was placed on both sides of a hemocytometer counting chamber covered with a glass coverslip, viewed under inverted fluorescence microscopy at 20X magnification using bright-field illumination. The total cell count in 1 mL was calculated by counting cells within the middle square (S1 and S2) surrounded by three lines on all sides and applying the formula: Total number of cells = 2 × (S1 + S2 + ... + Snn) × 104 × dilution factor. For long-term storage, one million cells were stored in a 10% DMSO solution overnight in an isopropanol chamber at -80°C, then transferred to a nitrogen tank for future use.

The MDA-MB-231 cells, also provided by the Molecular Biology and Genetics Department at Bilkent University, were cultivated in high-glucose Dulbecco's Modified Eagle Medium (DMEM) supplemented with 10% Fetal Bovine Serum (FBS), 1% Penicillin/Streptomycin (Pen/Strep) antibiotic, 1% Non-essential Amino Acids (NEAA), and 1% L-glutamine. Essentially, the cultivation procedures for both cell lines were similar except for the medium composition, which varied according to the specific cell line requirements.

2.8 Binding Assay

The method employed to establish the attachment of bacteria to JIMT1 involved a binding assay. The pZA mproD RFP CmR plasmid, responsible for facilitating the expression of red fluorescence protein, was introduced into *BL21* pET22b T7 lacO his 2Rs15d Ag43 AmpR bacteria. Upon induction of the double-transformed bacteria with 1 mM IPTG, they were centrifuged at 8000 rpm for 10 minutes, and subsequently, the media was removed. The resulting pellet was carefully re-suspended in 1X PBS under sterile conditions. In parallel, *E. coli BL21* (DE3) was also inoculated to serve as a control.

The JIMT1 cells, cultured in a T75 flask, underwent passaging, and approximately 10^5 cells were dispensed into each well of a 24-well plate containing 100 µl of Low Glucose DMEM without FBS and antibiotics. Within these wells, a glass slide was positioned at the base. Simultaneously, an equal number of HER2- CHO cells were placed in wells in a separate plate, functioning as a control. Approximately 10^7 bacteria were counted and subsequently added to each well containing the mammalian cells. These plates were then incubated for one hour at 37°C.

Following the incubation period, the glass slides were extracted, subjected to three washes with 1X PBS to eliminate any unbound bacteria, and then positioned on a drop of mounting solution atop a microscope slide. Visual documentation was acquired using a confocal microscope at a 20X dry setting to capture images of the bacterial attachment to the mammalian cells.

A workflow diagram of binding assay is provided below:

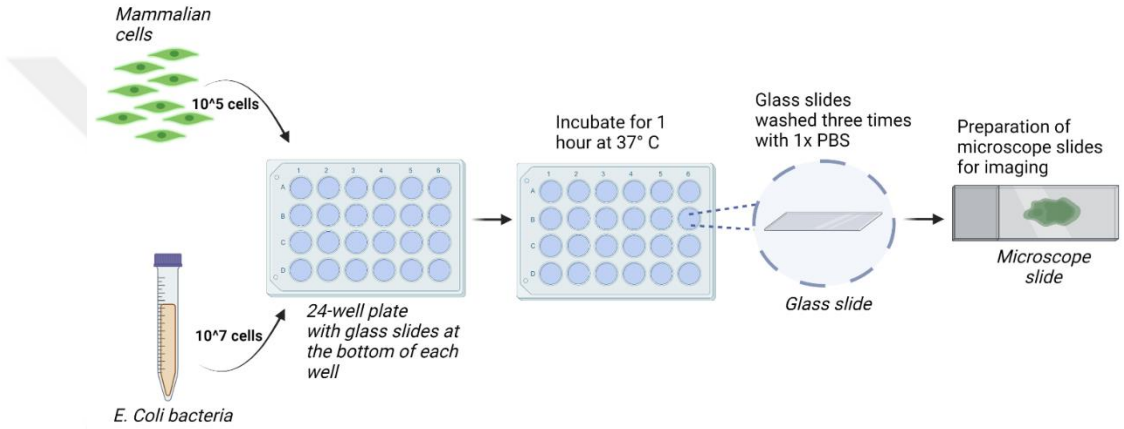

Figure 2: Workflow diagram for binding assay. Mammalian cells (JIMT1 and CHO) are seeded in a 24-well plate with each well containing a glass slide at the bottom. Bacteria *E. Coli BL21* and *E. Coli BL21* Nb is added to the wells after the mammalian cells have grown to 70% c confluency. After 1 hour of incubation with bacteria, the glass slides are removed from the bottom of wells with the help of tweezers. These are washed with sterile 1X PBS three times to remove any unbound bacteria. The glass slides are then inverted and placed at the center of microscopic slides on a drop of mounting solution. They are secured with the help of nail varnish. The slides can then be stored at 4ºC or imaged.

2.9 2D *in vitro* Assay

Mammalian cells, previously passaged and counted, were seeded at a density of 10^4 cells in 100 µL of growth media within a 96-well plate. These cells were incubated overnight at 37ºC and 5% CO2 to reach 80% confluency. Bacterial strains, including *E. coli BL21* (DE3), pZa native teto HlyE Yebf his - mScarlet CmR, and *BL21* pET22b T7 lacO his 2Rs15d Ag43 AmpR pZa native teto HlyE Yebf his CMR – mScarlet, were inoculated and induced using aTc and/or 1 mM IPTG. Following induction, the OD600 was measured to estimate the number of bacteria. An OD600 value of 1 corresponds to roughly 10^9 bacteria (*E. coli*) per mL.

The bacteria were then centrifuged at 8000 RPM at 4°C for 10 minutes, and the supernatant was removed. The resulting bacterial pellet was re-suspended in sterile 1x PBS. Wells containing the seeded mammalian cells were washed with 1X PBS, and the media was exchanged with 100 µL fresh DMEM devoid of Pen Strep and FBS. After appropriate calculations, 5*10^5 bacterial cells were added to the wells. The plate was incubated overnight at 37°C and 5% CO2.

The subsequent day, images were captured using a confocal microscope under a 20X dry setting to observe the interaction between the bacteria and the mammalian cells.

2.10 3D Cell Culture Spheroid Formation

To evaluate the effectiveness of our engineered bacteria within a 3D cell culture setup, we established mammalian cell spheroids using the agarose method. We prepared a 1.5% High Purity Agarose solution by blending 1.5 grams of high purity agarose powder in 100 mL of PBS, which was then sterilized via autoclaving. Subsequently, 100 µl of the agarose solution was dispensed into

wells of a 96-well plate and allowed to solidify for 1 hour. This forms a type of matrix over which cells coagulate when added to take on a spheroid formation.

Our cells, having reached 80% confluency in a T75 flask, were passaged and counted. Approximately 10,000-15,000 cells were added per well, adjusting the total volume to 100µl with fresh media devoid of Pen Strep and FBS. The cells were given a 3-day period to grow and form into spheroids. The cell number was arranged to form spheroids around 300-400µm in width. Initial images were captured before introducing bacteria into the wells. The workflow is illustrated below in Figure 2 in the next section.

2.11 3D *in vitro* Assay

The bacteria used in this experiment encompassed *E. coli BL21* - mScarlet, pZa native teto HlyE Yebf his - mScarlet CmR, and *BL21* pET22b T7 lacO his 2Rs15d Ag43 AmpR pZa native teto HlyE Yebf his CMR – mScarlet. These bacteria underwent inoculation, dilution, and induction processes. Following induction, the bacterial suspensions were centrifuged for 5 minutes at 8000 rpm and 4ºC. The resulting supernatant was discarded, and the pellet was re-suspended in sterile 1X PBS. Subsequently, 10^5 bacterial cells were introduced into each well of the relevant groups. Additionally, 0.3µl of aTc and IPTG were added to the pertinent wells. The plate was incubated at 37ºC, and the second set of images was captured after 4 hours. Further imaging sessions were conducted over the following two days (Figure 2). All images were acquired using a Leica confocal microscope at a 20X dry setting.

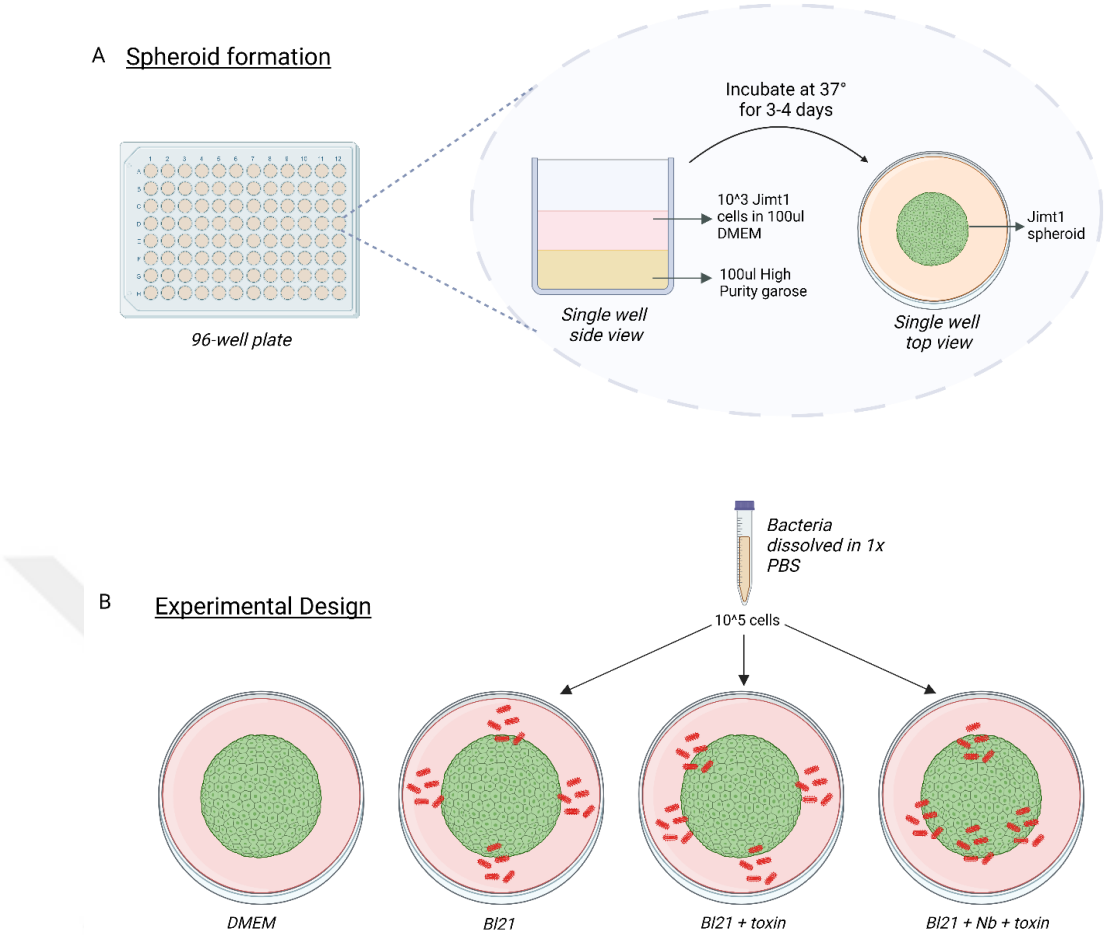

Figure 3: Protocol for Spheroid Experiment. (A) Spheroid Formation using High Purity Agarose: To create spheroids, 100 µl of high purity agarose was dispensed into each well within a 96-well plate, allowing it to solidify for one hour. Subsequently, ap approximately 10,000-15,000 JIMT1 cells were introduced per well, and the total volume was adjusted to 100 µl using Low-Glucose DMEM, excluding antibiotics. The cells were incubated for three days to foster spheroid development. (B) Replicated Groups for Experiment: Four replicate wells were established for distinct groups: DMEM, *E. Coli BL21* Wild-type (Wt), *E. Coli BL21* HlyE, and *E. Coli BL21* HlyE Nb. Bacteria, cultured in LB, were induced separately with aTc and IPTG. Post-induction, bacterial samples were

centrifuged at 8000 rpm for 5 minutes at 4ºC. The supernatant was removed, and the pellet was reconstituted in 1X sterile PBS. A total of 10^5 bacterial cells were added to the *E. Coli BL21* Wt, *E. Coli BL21* HlyE, and *E. Coli BL21* HlyE Nb groups, based on a conversion where an OD600 of 1 equates to 10^9 cells. No bacteria were introduced to the DMEM group. Imaging was conducted using a Leica confocal microscope before bacterial addition, 4 hours post-bacterial introduction (Day 1), on Day 2, and on Day 3.

The CellTiter-Glo 3D Cell Viability Assay protocol was followed according to the guidelines provided on the official Promega page. We set up opaque multi-well plates and transferred the contents from our 96-well plates. CellTiter-Glo® 3D Reagent was thawed overnight at 4ºC before use. The plate and its contents were allowed to equilibrate at room temperature (22–25°C) for about 30 minutes. The reagent was also warmed in water bath at 22ºC for 30 minutes. Subsequently, we added CellTiter-Glo® 3D Reagent in a volume equivalent to the amount of cell culture medium present in each well (e.g., for a 96-well plate, we added 100µl of CellTiter-Glo® 3D Reagent to 100µl of medium containing cells). We vigorously mixed the contents for 5 minutes to induce cell lysis, which was crucial for effective ATP extraction from 3D microtissues. The plate was then allowed to further incubate at room temperature for an additional 25 minutes to stabilize the luminescent signal. We recorded the luminescence using a microplate reader.

2.12 3-(4,5-Dimethylthiazol-2-yl)-2,5-diphenyltetrazolium bromide (MTT) assay

The MTT assay, based on 3-(4,5-Dimethylthiazol-2-yl)-2,5-diphenyltetrazolium bromide, was conducted to assess cell viability. In a 96-well plate, each well was seeded with an appropriate cell count, resulting in a final volume of 200 μL. Once the experimental period was completed, the medium from the wells was aspirated and substituted with 90 μL of fresh medium along with 10 μL of MTT solution (5 mg/mL in PBS).

The plates were then placed in an incubator for 4 hours at 37°C to enable the reduction of MTT and the formation of formazan crystals. Subsequently, the resulting formazan crystals were dissolved in 100 μL of DMSO, and the optical density was measured at 490/570 nm using a microplate reader.

2.13 Statistical Analyses

Statistical analyses graphs were created through GraphPad Prism 8.0 software. Multiple t-tests were executed for comparing the means of two groups. To compare the means of multiple groups with a single factor, one-way ANOVA was utilized, while for multiple groups with two factors, two-way ANOVA was employed.

For the analysis of 3D spheroid images, a total of four replicates of images from each day and group were analyzed using ImageJ software. In a concise process, initial adjustments were made for color thresholds using the LAB setting after establishing a global scale. The spheroid area was measured by employing the 'Analyze Particles' feature. A standardized adjustment of the threshold was implemented to eliminate noise based on image exposures. In cases where scattered cells were present on Day 3 in the *E. coli BL21* HlyE and *E. coli BL21* HlyE Nb groups, the 'Despeckle' setting was fine-tuned to ensure precision. After

recording the areas for each day, the outcomes were normalized by calculating the percentage area in comparison to the original spheroid area.

CHAPTER III: RESULTS AND DISCUSSION

3.1 Engineering *E. Coli Bl21* Bacteria to Target Breast Cancer Cells

In our experimental procedures, the *Bl21* strain of *E. coli BL21* was selected due to its amenability to genetic engineering, providing a favorable platform for our investigations. For the specific binding of these engineered bacteria to target cells, we employed a nanobody (Nb) designed to interact with HER2+ receptors present on breast cancer cells. The extensive evaluation of the 2Rs15d nanobody's binding affinity and specificity with HER2 receptors, both in controlled laboratory environments (*in vitro*) and within living organisms (*in vivo*), has been well-documented in previous studies[49].

To facilitate the attachment of *E. coli BL21* to the receptors on mammalian cells, we utilized a strategic approach involving the display of the nanobody on the bacterial surface. Achieving this involved leveraging the Ag43 autotransporter protein system, a proven method demonstrated to effectively present proteins on the surfaces of bacterial cells. This system, utilizing a specific signal peptide, has been previously validated in literature for its capacity to successfully display proteins on the outer surface of bacterial cells[47].

The introduction of the nanobody onto the surface of the *E. coli BL21* strain represents a crucial step in our experimental design, allowing for a targeted interaction between the bacteria and the HER2+ receptors on breast cancer cells. The utilization of the Ag43 autotransporter system in this context provides a robust and validated methodology for displaying the required nanobody, thereby

enabling a more precise and efficient binding of the engineered bacteria to the specific target receptors on the breast cancer cells' surface. This strategic approach laid the foundation for our subsequent investigations focused on the targeted interaction and potential therapeutic applications within the context of breast cancer.

3.1.1 Ag43 Cell Surface Expression System

To enable the expression of the nanobody on the surface of *E. coli*, the Ag43 autotransporter protein was employed. This protein utilizes the Type V secretion pathway to transport the desired protein to the outer surface of the *E. coli* bacterial cells. Structurally, the Ag43 protein includes components such as an N-terminal signal sequence (pelB), a passenger domain, as well as alpha and beta subunits. The protein of interest, in this case, the nanobody, is inserted into the system alongside the N-terminal signal sequence. The display process involves a two-step pathway: initially, the protein is secreted into the periplasm through the SecYEG translocon 23, and subsequently, beta barrels are formed and integrated into the outer membrane of *E. coli*. This process ultimately leads to the expression of the nanobody on the surface of the *E. coli* cells

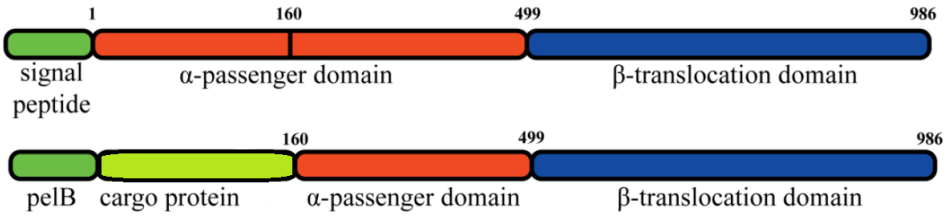

Figure 4: Schematic representation of Ag43 autotransporter protein domains.

3.1.2 Cloning of pET22b T7-LacO pelb 2Rs15d Ag43 AmpR

The 2Rs15d nanobody was inserted downstream of the T7 LacO promoter into a pET22b vector. The base structure of this vector was derived from the pET22b Ag43 160N 6h sfGFP AmpR plasmid, provided by Recep Erdem Ahan, a fellow member of our laboratory and a collaborator on this project. This vector contained an Ag43 secretion cassette designed to facilitate the nanobody's expression on the surface of *E. coli* cells. Additionally, a signal peptide (pelB) was utilized to guide the nanobody to the periplasmic space within the bacterial cell.

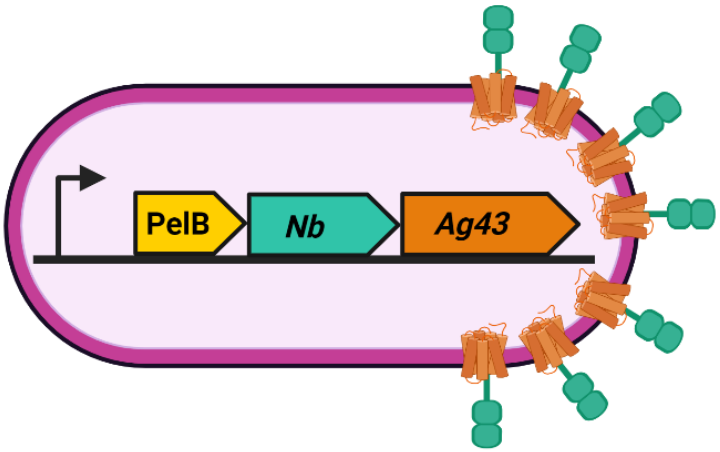

Figure 5: Surface display of 2rs15d Nanobody (Nb) on *E. coli* bacteria via Ag43 autotransporter protein system.

3.1.3 Expression Verification of Surface Displayed Nanobody (Nb)

We performed immunocytochemistry (ICC) experiment, as explained in materials and methods section, to verify surface expression of the nanobody on bacteria surface. We performed this using 2Rs15d tagged with DyLight 550,

which produces red fluorescence. When visualized under the microscope, if bacteria appear red it means that it displays Nb on its surface. Lack of red color would indicate bacteria did not successfully display the Nb. Our ICC image shown below (Figure 6), taken with inverted fluorescence microscope, shows successful surface display of 2Rs15d Nb.

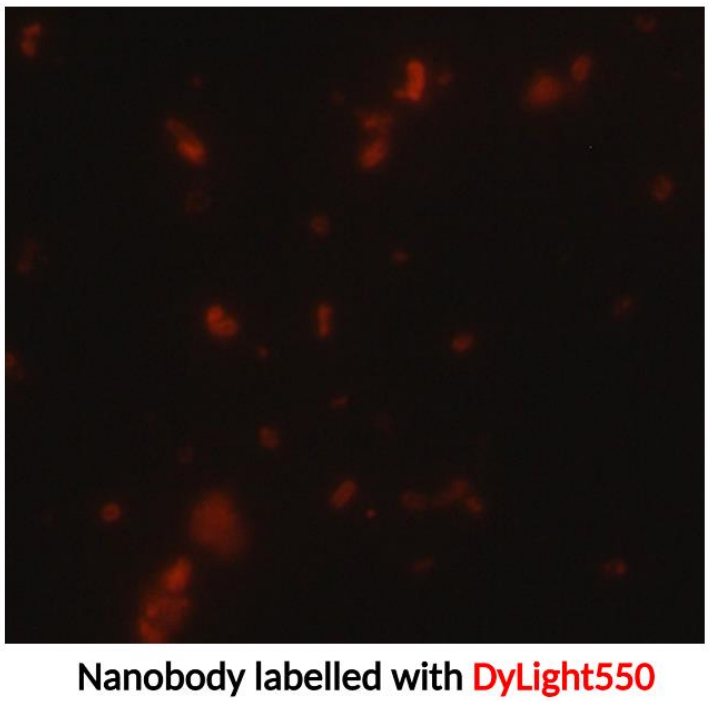

Figure 6: Immunocytochemistry image showing Nb on bacteria tagged with DyLight 550, giving red fluorescence.

We also performed a Western Blotting experiment to verify expression of Nb. The relevant band (~40 kDa) is shown in Figure 5.

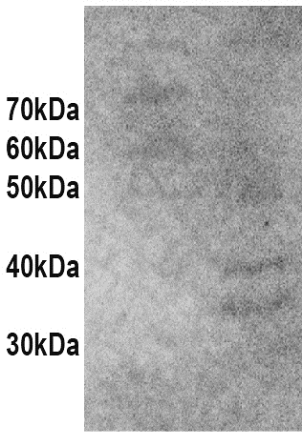

Figure 7: Western Blotting done to verify presence of 2Rs15d Nanobody (Nb) in engineered bacteria, *E. Coli* Nb. The relevant band is seen at ~40 kDa

3.1.4 Assessment of Nanobody Binding to Targeted JIMT1 Cells

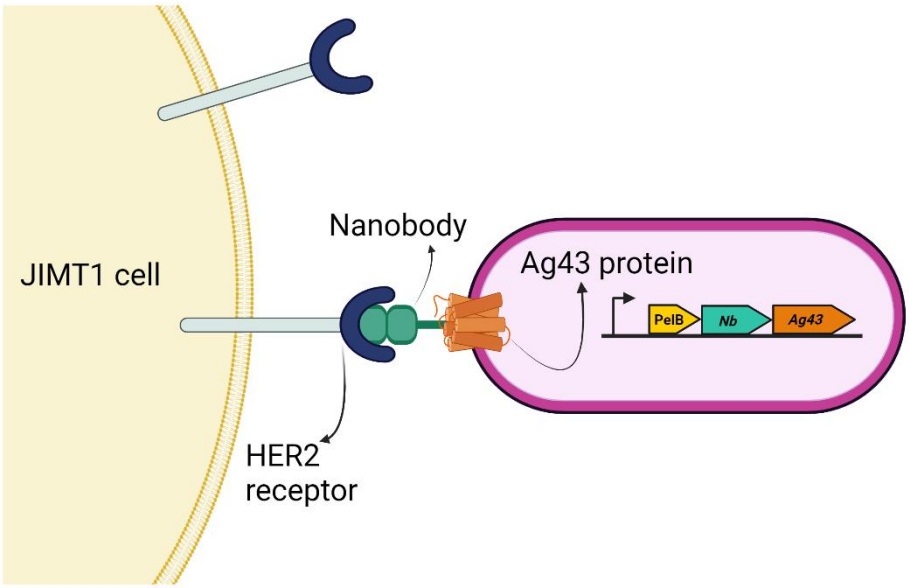

Figure 8: Diagrammatic illustration made using Biorender.com to show binding of surface-displayed Nb on *E.coli* to HER2 receptors on JIMT1 breast cancer cells.

Our hypothesis posits that these bacterial cells will adhere to JIMT1 mammalian

breast cancer cells due to the heightened expression of HER2 receptors in JIMT1. To examine this, we conducted a binding assay, using CHO-K1 cells as a negative control. Both *E. coli BL21* and *E. coli BL21* modified with surface-displayed nanobody (*E. coli BL21* Nb) were incubated with CHO and JIMT1 cells placed in a well-plate with glass slides at the base. Following a one-hour incubation, the slides were washed with PBS to eliminate any unbound bacteria. Confocal microscopy images reveal CHO cells (blue) without any attached *E. coli BL21* or *E. coli BL21* Nb. While JIMT1 cells (green) exhibit no binding of *E. coli BL21*, the presence of *E. coli BL21* Nb (red) adhering to JIMT1 cells confirms our hypothesis.

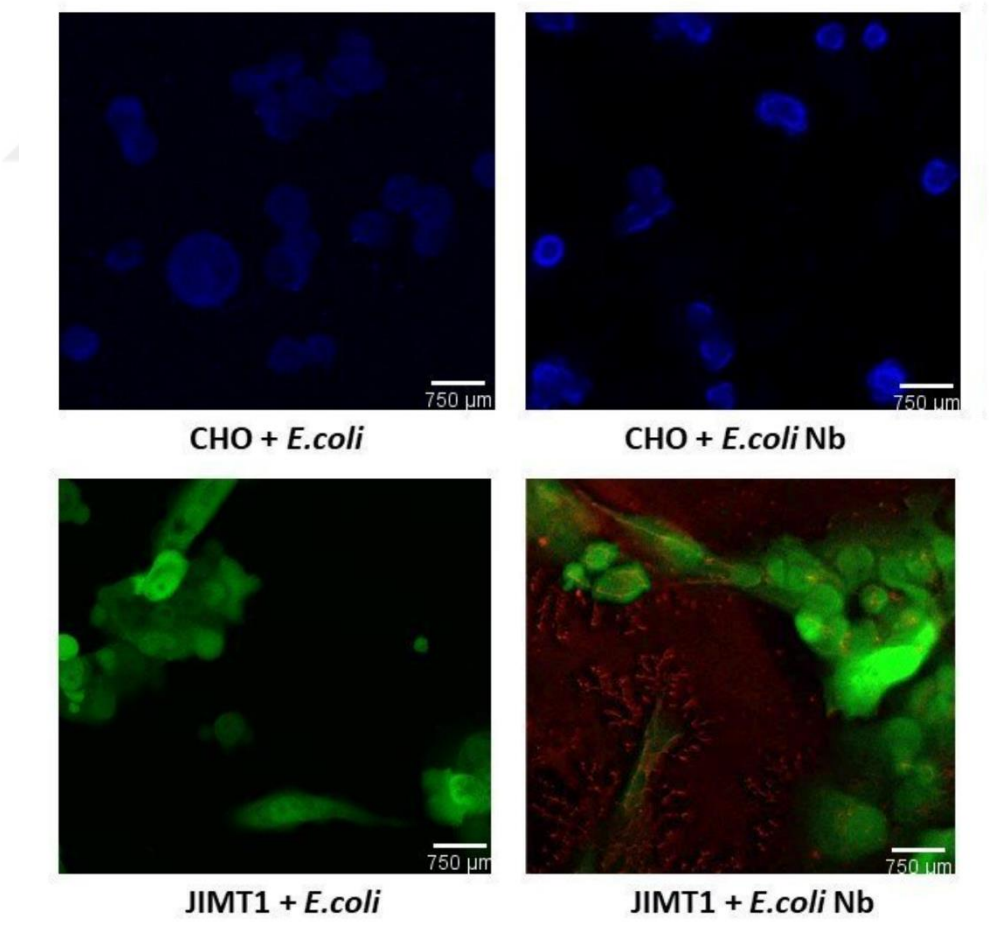

Figure 9: The binding assay aimed to confirm the adherence of *E. coli BL21* Nb to

JIMT1 cells. *E. coli* was genetically modified with pZA mproD RFP to express red fluorescence. As control, HER2- CHO cells (blue) revealed no interaction with either *E. coli BL21* or *E. coli BL21* Nb bacteria. *E. coli BL21* exhibited no attachment to JIMT1 cells (green). In contrast, *E. coli BL21* Nb, displaying red fluorescence, was observed to be adhering to JIMT1 cells in the fourth group, attributable to the presence of the nanobody.

3.2 Elimination of JIMT1 Cells Using Hemolysin E (HlyE) Toxin

For our choice for the therapeutic agent, we decided to use the pore-forming Hemolysin E (HlyE) toxin, which has been shown to exert a cytotoxic effect towards mammalian cells. We engineered *E. coli BL21* to secrete HlyE toxin through the YebF secretion system. YebF secretion system is a type VI secretion system, known for its ability to secrete various proteins and compounds. This setup allowed us to have a controlled release of the HlyE toxin, using its cell-killing potential to eliminate the breast cancer cells.

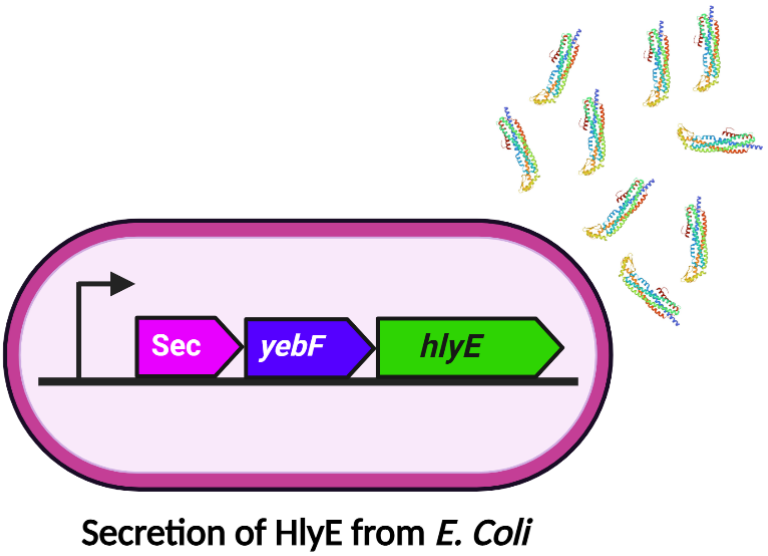

Figure 10: *E. coli BL21* design for secretion of HyE using YebF secretion system.

3.2.1 Assessing the Cytotoxic Effects of HlyE on JIMT1 Cells

We initially purified the HlyE protein using FPLC to assess its potential as a toxic agent against JIMT1 cells. We verified the purification through SDS-PAGE, observing the expected band at around 55 kDa.

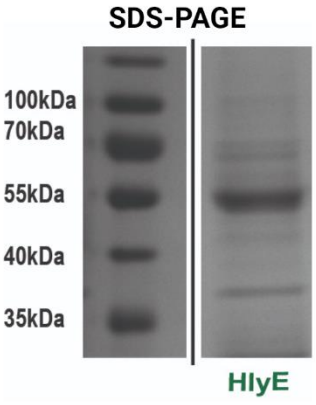

Figure 11: SDS-Page to show purified HlyE protein band at 55kDa.

To investigate the impact of the purified HlyE on our JIMT1 cell line, we

introduced three different HlyE concentrations (750 ng/µl, 1200 ng/µl, and 2000 ng/µl) to mammalian cells seeded in a 96-well plate. As a negative control, we added 50 µl of 1X PBS. After the treatment, we captured images using an inverted fluorescence microscope.

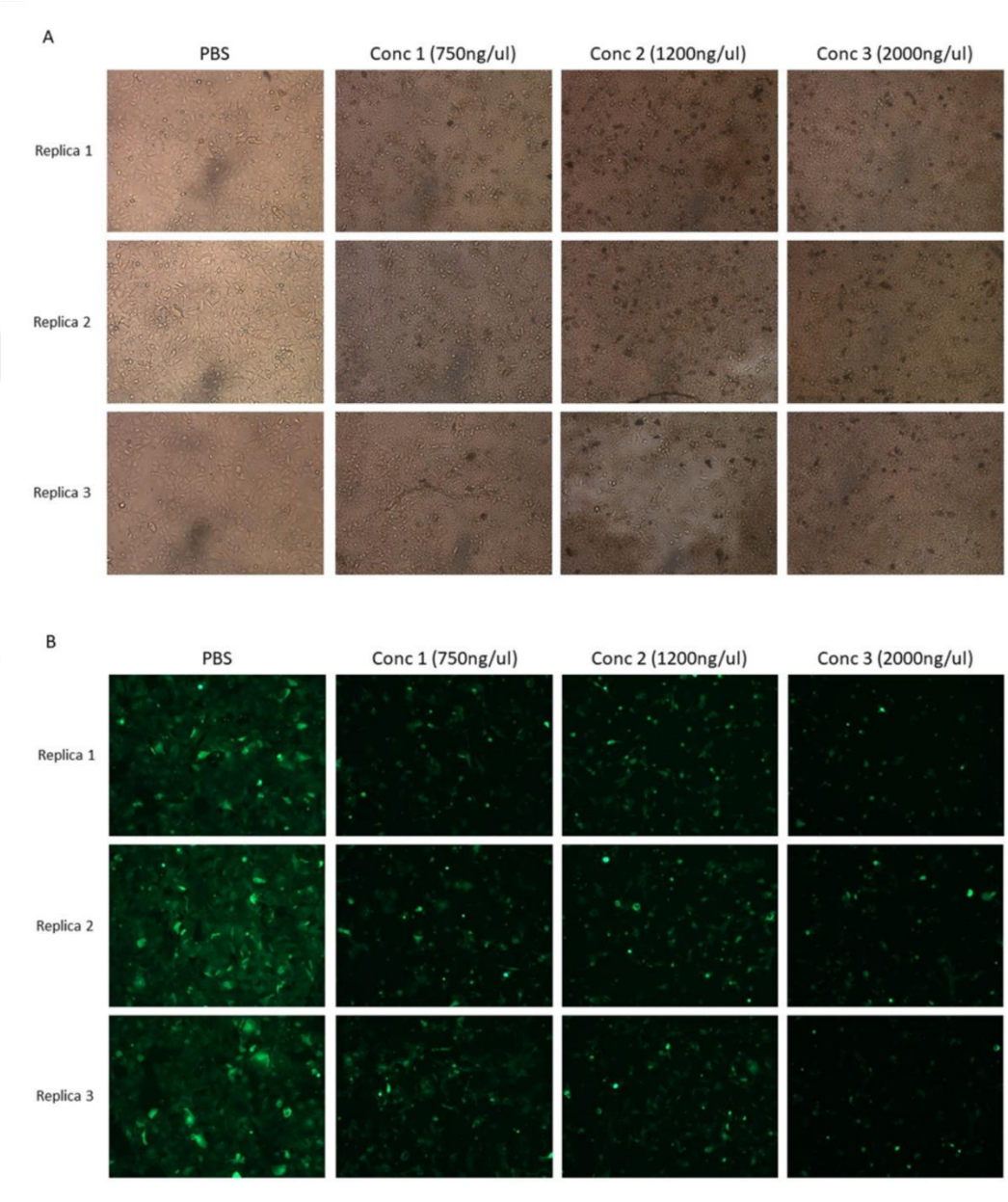

Figure 12: Analyzing HlyE Toxicity in JIMT1 Cells: Images captured using an inverted fluorescence microscope exhibit the impact of escalating concentrations of purified HlyE on JIMT1 cells. A total of 10^4 JIMT1 cells were seeded and allowed to grow overnight within a 96-well plate. Each of the four groups,

including the PBS (control), Conc 1 (750 ng/µl HlyE), Conc 2 (1200 ng/µl HlyE), and Conc 3 (2000 ng/µl HlyE), had three replicate wells imaged. Subsequently, 50µl of each concentration was added to the respective wells containing JIMT1 cells, followed by an overnight incubation of the well-plate. Images were captured in both bright-field (A) and fluorescent (B) settings. These images illustrate a consistent reduction in JIMT1 cells as the concentration of HlyE increases, affirming its toxic impact.

Following incubation, we conducted MTT assays to evaluate cell viability, revealing a significant decrease in JIMT1 cells treated with HlyE, especially at higher concentrations compared to those treated with PBS (Figure 13). These results strongly support the potential of the HlyE toxin as an effective therapeutic agent against breast cancer cells.

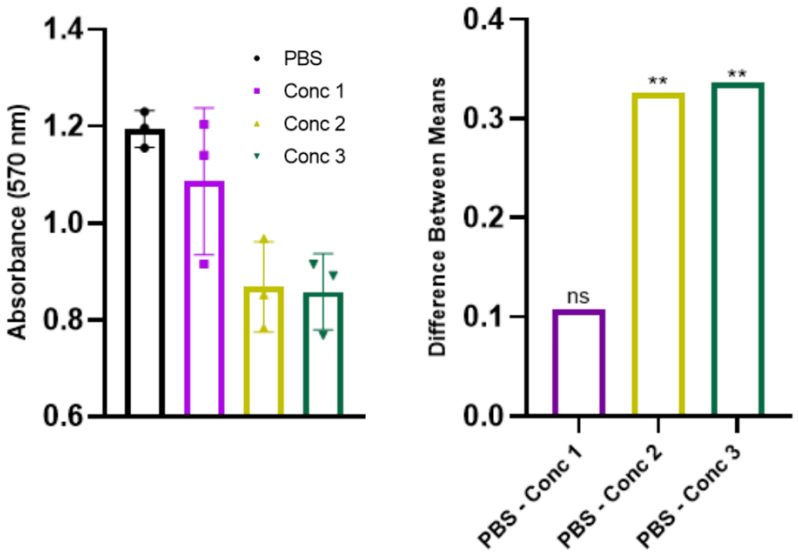

Figure 13: The purified HlyE protein, along with the PBS (control), is introduced to JIMT1 mammalian cells at varying concentrations (Conc 1 = 750ng/µl, Conc 2 = 1200ng/µl, Conc 3 = 2000ng/µl) to evaluate the lethal effects of HlyE on the

cells. The assessment of purified HlyE cytotoxicity was conducted using the MTT (3-[4,5-dimethyl-2-thiazolyl]-2,5-diphenyl-2H-tetrazolium bromide) assay, measuring absorbance at 570nm. The initial graph portrays cell viability within the four groups: PBS, Conc 1, Conc 2, and Conc 3. The subsequent graph illustrates the One-way ANOVA analysis of the MTT results, displaying a significant (**) distinction between the mean cell viability of PBS and Conc 2 + Conc 3.

3.2.2 HlyE Secretion from *E. Coli BL21*

We engineered *E. Coli* bacteria to secrete HlyE toxin as shown in Figure 10. We opted to employ the pTetO native promoter, known for its bidirectional nature. This decision aimed to regulate the expression of our specific protein and TetR concurrently, allowing us to utilize this design within *E. coli BL21* (DE3) in an inducible manner. Within this system, we chose to implement the YebF secretion mechanism for the external release of our toxin. Following the cloning of the parts, we executed the Gibson Assembly method and chemically transformed the resulting product into *E. coli* PRO DH5α. Once validated through colony PCR, confirming the accuracy of the cloning process, two colonies were sent for sequencing. Upon confirmation via sequencing, the accurate plasmid was chemically transformed into *E. coli BL21* (DE3). To concentrate the supernatant samples, we utilized the TCA protein precipitation technique. Subsequent to the cloning and sequencing of our bacteria, a Western Blot analysis was performed to examine the supernatant for the presence of HlyE using the TCA precipitation method, revealing the expected band at approximately 40 kDa.

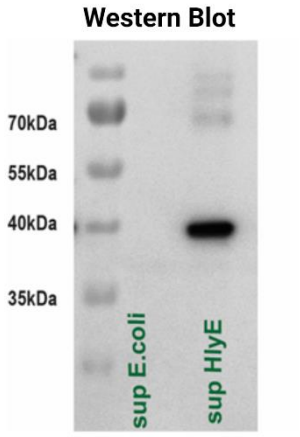

Figure 14: Western Blot for verification of secretion (HlyE band ~40kDa) is done by using supernatant samples concentrated by TCA precipitation.

3.2.3 Testing HlyE Secreting Bacteria on JIMT1 Cells

Supernatant of HlyE secreting bacteria was tested on JIMT1 cells. Equal volumes of supernatant from *E. coli BL21* (control) and *E. coli BL21* HlyE were incubated overnight with JIMT1 cells seeded in a 96-well plate. A cell viability assay using MTT was performed the next day, results are shown in Figure 15.

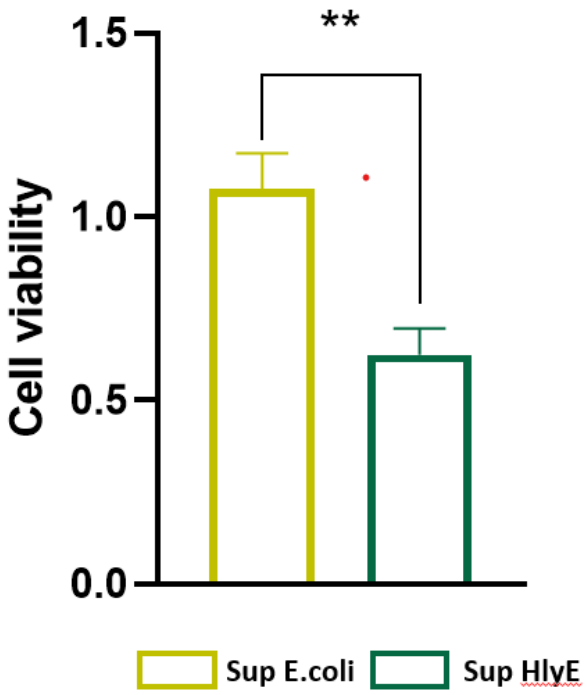

Figure 15: MTT to compare JIMT1 cell viability after adding supernatants of *E. coli BL21* and *E. coli BL21* HlyE. Results show a significant difference (**) between cell viability of the two groups.

3.3 Testing the Effects of our Proposed Engineered Design *E. coli BL21* HlyE Nb on JIMT1 Breast Cancer Cells

The primary goal of this research was to utilize genetic engineering methods to develop a new bacterial structure that combines the surface-expressed Nb with the HlyE secretion pathway effectively (Figure 16). This integrated system aims to provide synergistic advantages, utilizing the specific binding capability of the Nb to selectively target and attach to JIMT1 cells. Subsequently, the secretion of HlyE is expected to perform the eradication of the target cells.

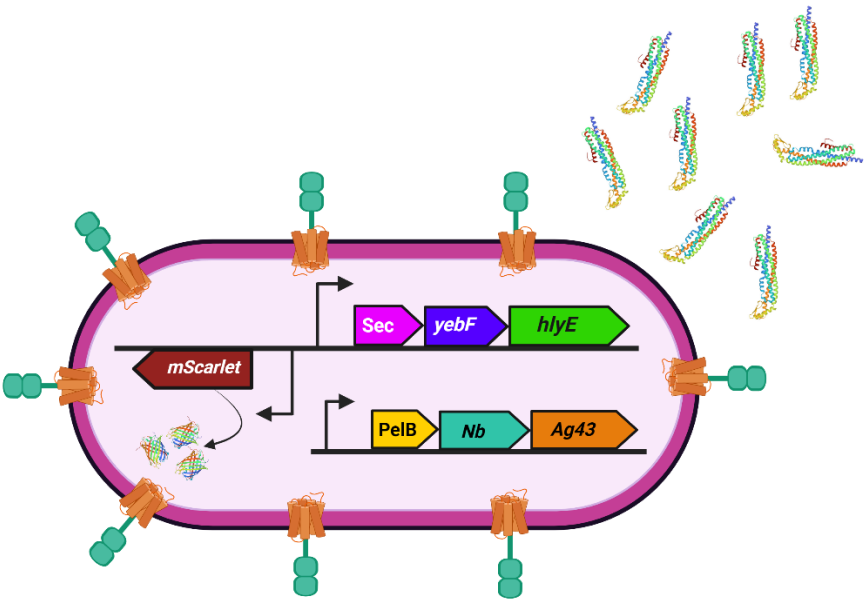

Figure 16: *E. coli* with surface-displayed Nb and HlyE secretion

3.3.1 Expression Verification of Nb Display and HlyE Secretion

To validate the successful expression of the targeted proteins in our engineered *E. coli BL21*, we conducted a comprehensive assessment employing Western Blotting techniques. This experiment involved the analysis of both Whole Cells (WC) and supernatants (sup), with unmodified *E. coli BL21* serving as a control for comparison, as illustrated in Figure 17. The incorporation of mScarlet into the bacterial system was undertaken strategically to augment contrast and facilitate optimal visualization during subsequent imaging experiments. This meticulous validation process ensures the reliability and accuracy of our engineered *E. coli BL21* as we proceed with further investigations in this study.

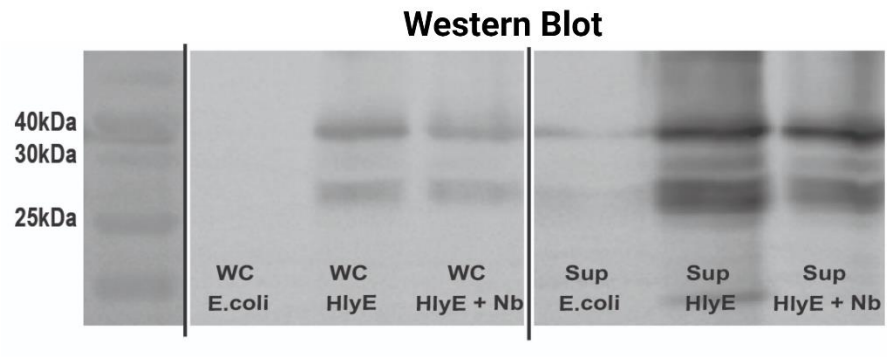

Figure 17: Western Blot with whole cell (WC) and supernatant (Sup) concentrated with TCA precipitation showing bands at 40kDa for HlyE in all engineered bacteria cells.

3.3.2 2D Assay with JIMT1 and Engineered *E. coli*

To investigate the in vivo effects of the bacteria, we opted for a 2D cell culture experiment as part of our rigorous analysis. JIMT1 cells, cultured with the standard growth medium DMEM, and those cultured with unaltered *E. coli BL21* Wild-type (Wt) served as our negative controls. To assess the effectiveness of our double-transformed bacterial strain, we introduced an *E. coli BL21* secreting HlyE group into the experiment. This allowed us to determine whether *E. coli BL21* HlyE Nb indeed facilitates a more targeted release of HlyE compared to *E. coli BL21* HlyE, resulting in a more pronounced reduction in JIMT1 cells. The experimental procedure involved seeding mammalian cells in a 96-well plate and overnight incubation with the relevant bacteria, along with the addition of media. Confocal microscopy images taken the following day revealed negligible differences in mammalian cells in the *E. coli BL21* Wt group compared to those growing in DMEM. A more significant difference was observed in the *E. coli*

BL21 HlyE group, while the most noticeable disparity, both in terms of quantity and morphology of JIMT1 cells, was observed in the *E. coli BL21* HlyE Nb group. In the confocal images shown in Figure 18, JIMT1 cells, stably transfected with GFP, appear in green, while bacteria expressing mScarlet are visible in red.

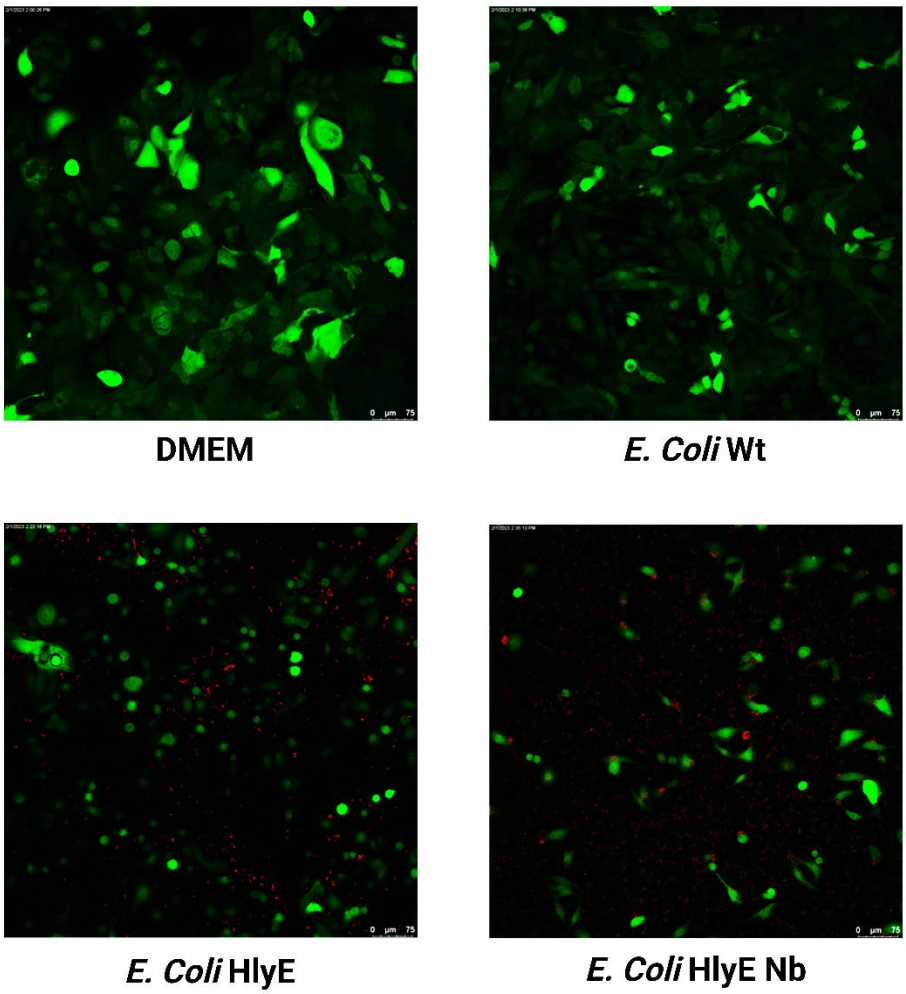

Figure 18: 2D assay experiment was conducted using green fluorescent JIMT1 cells and red fluorescent bacteria. The images captured depict JIMT1 cells under normal conditions in DMEM, one day after incubation with *E. coli BL21* (control), and subsequent to incubation with *E. coli BL21* HlyE and *E. coli BL21* HlyE Nb. Notably, the experiment reveals evident cell death in the JIMT1 cells within the experimental groups, particularly following exposure to *E. coli BL21* HlyE Nb.

3.3.3 Comparison with Triple-Negative Breast Cancer Cell Line MDA-MB-231

To enhance the robustness of our findings, we introduced a control cell line, MDA-MB-231, representing triple-negative breast cancer cells that lack HER2 receptors. The selection of this control cell line was deliberate, given that our engineered bacteria leverage a HER2-targeting nanobody. Previous studies have extensively investigated the HER2 expression levels in both JIMT1 and MDA-MB-231 cell lines. Immunohistochemistry results have revealed that JIMT1 exhibits overexpression (3+) of HER2 with approximately 20-30 copies per cell[51], while the triple-negative MDA-MB-231 cell line demonstrates minimal to no expression of HER2 (0-1+)[52].

In parallel with the treatment administered to the JIMT1 cell line, MDA-MB-231 cells were exposed to the same bacteria, and we conducted a comprehensive comparative analysis. Figure 19 illustrates the identical 2D assay performed with MDA-MB-231 cells.

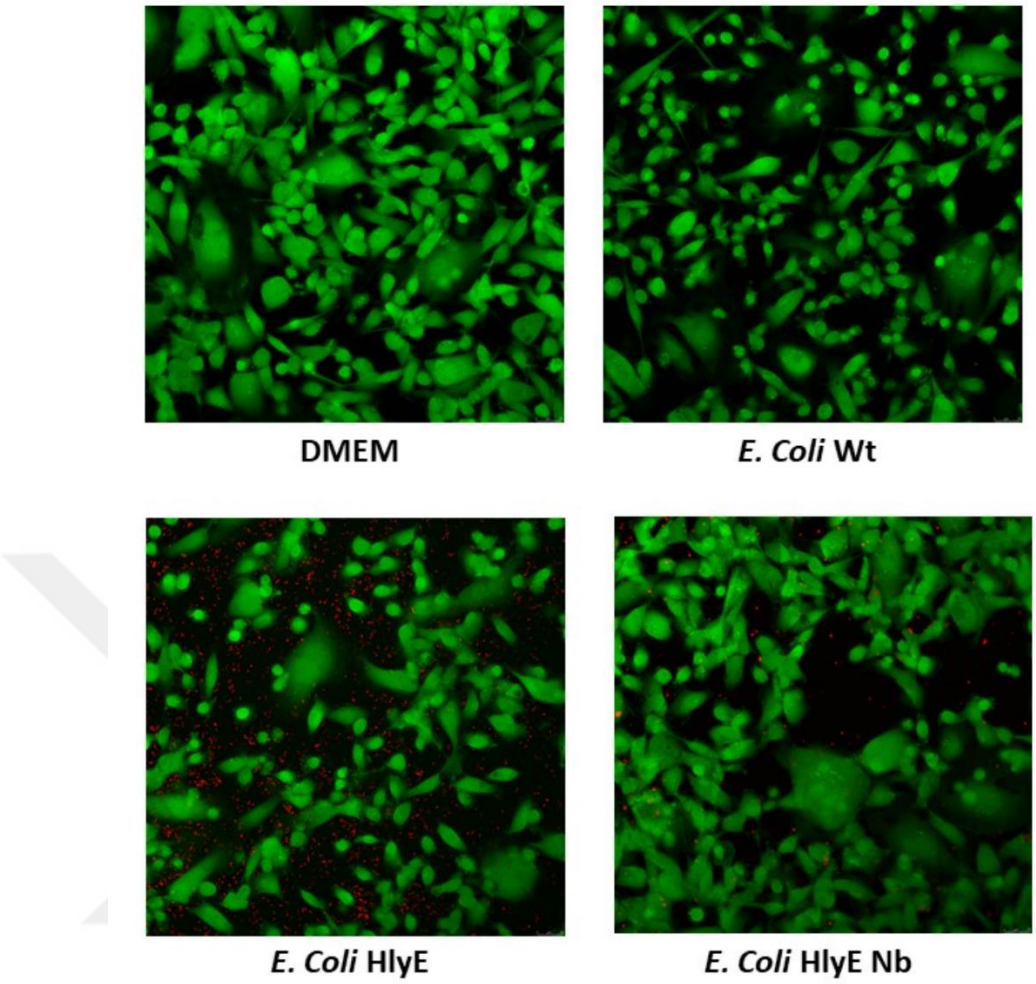

Figure 19: 2D assay with triple-negative MDA-MB-231 cells.

Notably, in Figure 19, we observed a significant contrast in the 2D assay images of MDA-MB-231 cells compared to those of JIMT1 (refer to Figure 18). There was little to no change in cell viability of the triple-negative cell line. This deliberate inclusion of a HER2-negative control cell line further strengthens our understanding of the specific targeting and cytotoxic effects of our engineered bacterial strain on HER2+ breast cancer cells.

Subsequent to eliminating bacteria in the wells with Gentamycin, we conducted an MTT assay to assess cell viability. The quantification of these results involved

a one-way ANOVA, utilizing *E. coli BL21* Wt as the designated control group. The findings for JIMT1 revealed a non-significant difference between *E. coli BL21* Wt and *E. coli BL21* HlyE, while a substantial difference was observed between *E. coli BL21* Wt and *E. coli BL21* HlyE Nb (*). Conversely, in the case of MDA-MB-231, there was no statistically significant difference observed between the *E. coli BL21* and *E. coli BL21* HlyE Nb groups. These outcomes contribute valuable insights into the specific cytotoxic effects of our engineered bacterial strain on the targeted JIMT1 cells, further highlighting the efficacy of our genetic modifications in inducing the desired response.

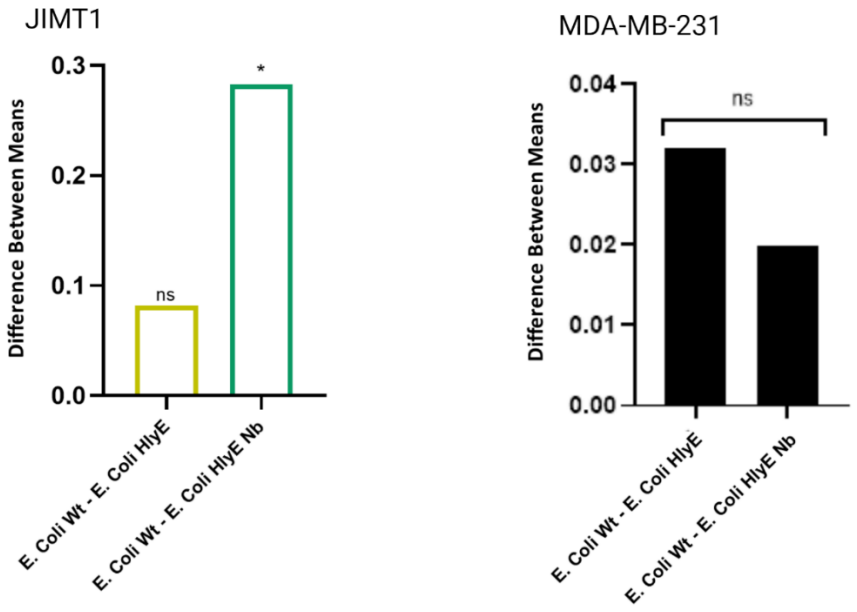

Figure 20: MTT ANOVA graphs to quantify and compare 2D Assay results of JIMT1 and MDA-MB-231.

3.3.4 Comparison Between *E. coli* HlyE and *E.coli* HlyE Nb

To justify the selection of 5 x 10^5 bacterial cells per well for the targeted eradication of JIMT1 cells, we conducted a titration dose experiment. This

involved systematically varying bacterial concentrations from 5 x 10^3 to 5 x 10^7 in tenfold increments. The primary aim was to identify the optimal bacterial dosage for maximal effects and to compare treatment outcomes for JIMT1 with *E. coli BL21* HlyE and *E. coli BL21* HlyE Nb. Following the experiment, confocal images were captured for each of the five dosage groups as shown below in Figure 21.

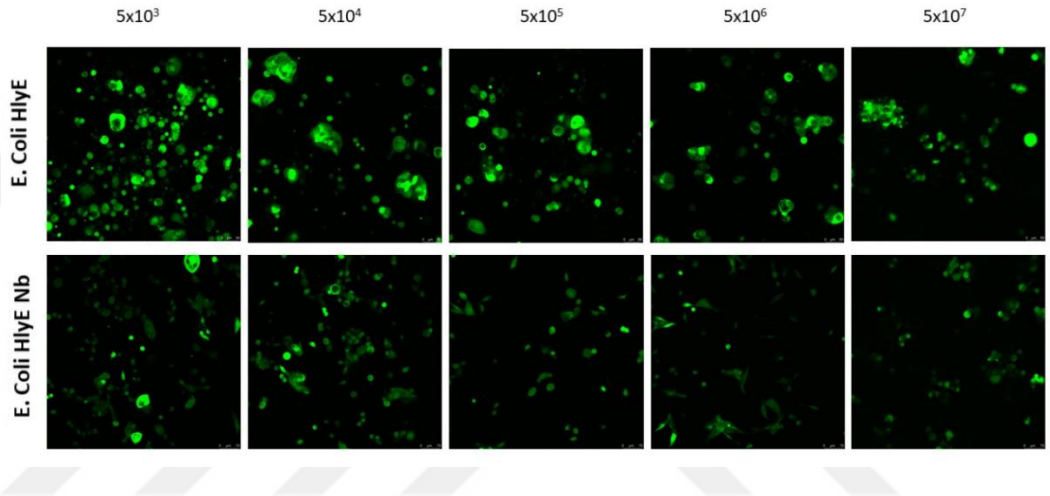

Figure 21: Dose-dependent experiment done to verify effects of increasing bacteria dosage on JIMT1 cells and comparison between *E. coli BL21* HlyE and *E. coli BL21* HlyE Nb. Numbers indicate bacteria cells added per well.

For a quantitative assessment of the impact, three replicate images from each concentration were analyzed using the Analyze Particles feature of ImageJ. Subsequently, a two-way ANOVA was conducted to evaluate dose-dependent effects on JIMT1 with increasing concentrations of *E. coli BL21* HlyE and *E. coli BL21* HlyE Nb. The ANOVA results (see Figure 22) indicate a significant difference in viable JIMT1 cells between the two groups at lower concentrations (5 x 10^3 – 5 x 10^5), with *E. coli BL21* HlyE showing relative ineffectiveness. At higher concentrations, the difference becomes non-significant; however, high

bacterial concentrations prove lethal, as the bacteria tend to dominate the well, rendering their presence redundant.

In the *E. coli BL21* HlyE Nb group, a gradual decline in JIMT1 cell count is observed in the first two groups, followed by a remarkable reduction upon employing 5 x 10^5 bacteria cells. This reduction remains consistently pronounced in the subsequent two groups, rendering the addition of higher bacterial quantities unnecessary and potentially hazardous. This optimization minimizes the concentration of *E. coli BL21* HlyE Nb bacteria needed to effectively eliminate JIMT1.

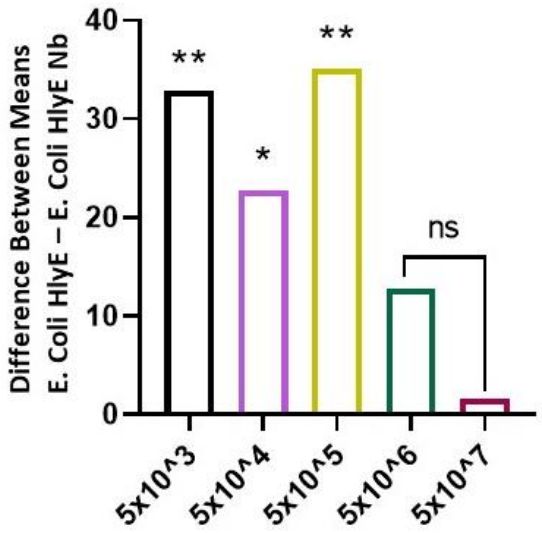

Figure 22: Two-way ANOVA to compare dose-dependent effects on JIMT1 of *E. coli BL21* HlyE and *E. coli BL21* HlyE Nb.

Conversely, *E. coli BL21* HlyE alone would require a larger dose, potentially causing hazardous effects at such high concentrations, and leading to bacterial dominance in the wells. Our findings underscore the significance of the chosen bacterial concentration (5 x 10^5 cells) as an optimal balance between efficacy and

safety in targeting and eliminating JIMT1 cells. This highlights the effectiveness of our bacterial design with surface-displayed nanobodies for targeted elimination, requiring fewer bacteria and demonstrating greater efficacy in killing JIMT1 cells.

3.4 3D Cell Culture Spheroid Experiments

Upon meticulous examination, we determined that relying solely on a singular assay proved insufficient for gauging the efficacy of our system. To enhance the robustness of our hypothesis and replicate the intricate environment of a tumor cell mass, we chose to perform 3D cell culture experiments, specifically generating JIMT1 cell spheroids. 3D cell culture spheroids, unlike conventional 2D cultures, constitute a sophisticated model marked by heightened physiological relevance and complexity. Unlike 2D monolayers, 3D cell culture spheroids consist of cell clusters capable of establishing intricate cell-cell and cell-matrix interactions, leading to improved cell differentiation, proliferation, and survival—characteristics that more closely mirror the *in vivo* microenvironment of a tumor mass[53]. Therefore, utilizing cell spheroids presented a more superior and biologically relevant approach for our study.

The preparation of JIMT1 cell spheroids employed the high-purity agarose method, wherein the bottom of wells in a well-plate was initially filled with high-purity agarose, creating a concave hydrogel. Upon introducing cells, they tended to aggregate at the center, forming a spheroid through cell-cell and cell-matrix interactions (Figure 3). Spheroids with diameters ranging from 300-500 μm were cultivated over a three-day incubation period. Previous research has established

that the stability of bacterial spheroid co-cultures endures for a maximum of two weeks[53]. This limitation arises from disparate growth rates between bacteria and mammalian cells, with the bacterial population outpacing the replenishment of culture medium nutrients. Consequently, this renders the system unsustainable for mammalian cells beyond the specified two-week timeframe.

3.4.1 3D Assay with JIMT1 and MDA-MB-231 Spheroids

Similar to the 2D assay experiment, we formed cell spheroids which were divided into four difference treatment groups: DMEM, *E. coli BL21*, *E. coli BL21* HlyE and *E. coli BL21* HlyE Nb. A pictorial representation of the four treatment groups is given below:

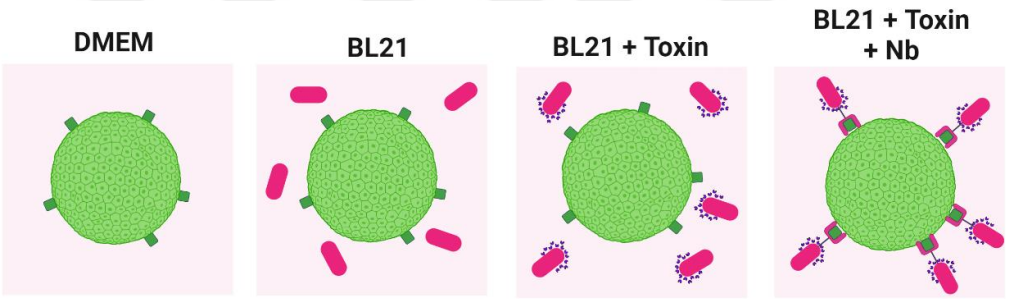

Figure 23: Diagram showing the four treatment groups for mammalian cell spheroids. DMEM and *E. coli BL21* are control groups. Bacteria releasing toxin is represented in the third group *E. coli BL21* HlyE. And the fourth group *E. coli BL21* HlyE Nb shows bacteria releasing toxin bound to spheroid due to the presence of nanobody, hypothesized to promote a more targeted toxin release.

Confocal microscopy was employed to capture images both prior to bacterial introduction to the wells, once spheroid formation had occurred, and subsequently for comparative analysis with the spheroid's initial state. Following

spheroid formation, bacteria were introduced, and images were acquired at four hours post-incubation (day 1), the subsequent day (day 2), and a final set on day 3. Figure 24 illustrates the progression of bacterial spread and the concomitant reduction in spheroid area. Confocal overlay images depict JIMT1 cells in green, bacteria in red, and black spots representing dead JIMT1 cells.

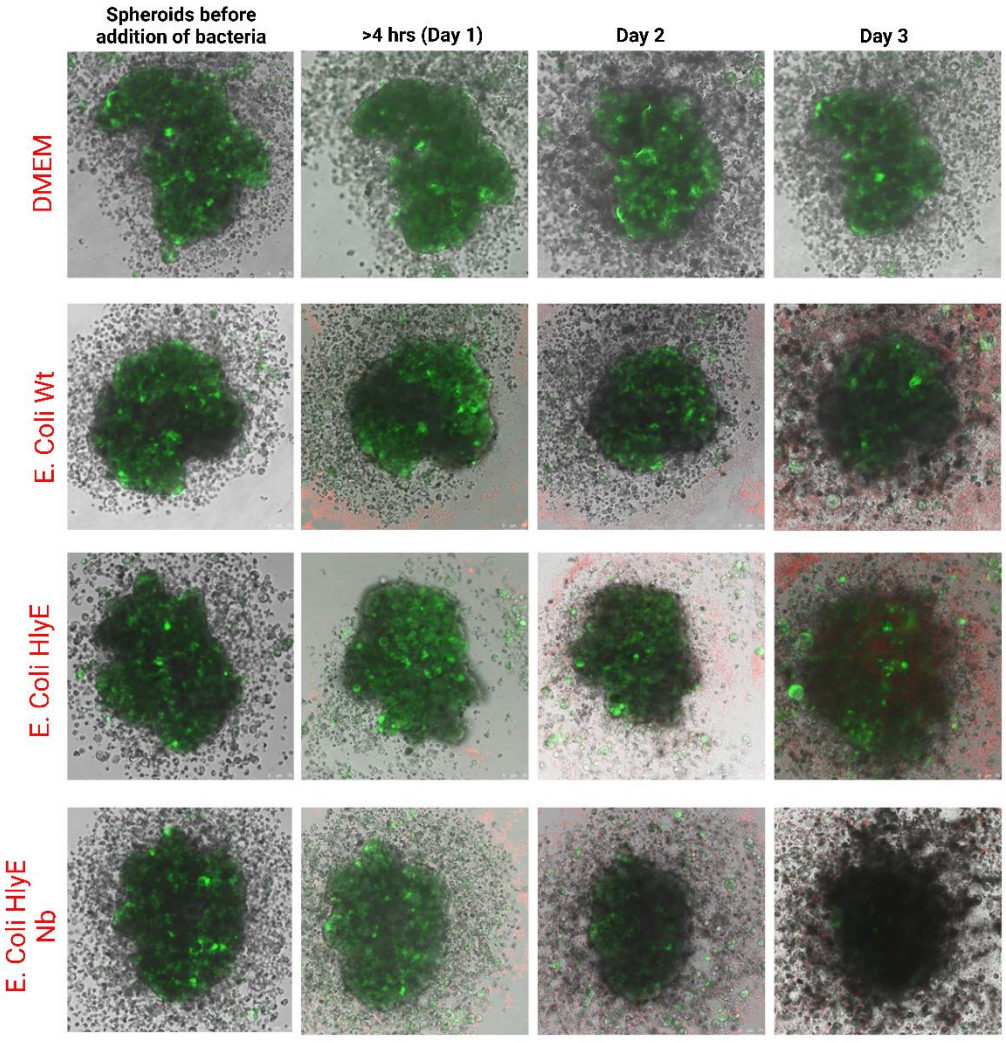

Figure 24: Confocal microscopy images of JIMT1 spheroids experiment.

Notably, a marginal reduction in spheroid size was observed in wells containing DMEM alone without bacteria. Similarly, spheroids treated with non-engineered

E. coli BL21 exhibited a gradual, albeit modest, decrease over the experimental duration. In contrast, spheroids treated with *E. coli BL21* HlyE exhibited a substantially more pronounced alteration; by day 3, the spheroids had lost their clustered formation, displaying evident disruption with a considerable decrease in viable (green) JIMT1 cells compared to the experiment's onset. Observable changes were apparent as early as day 2 in this instance. The most substantial decrease in spheroid area and the transition of JIMT1 cells from a spheroidal configuration to dispersed cells were observed in the JIMT1 group treated with *E. coli BL21* HlyE Nb over the three-day period. Despite HlyE's known potency as a toxin for mammalian cells, our 3D cell culture experiment revealed that the surface-displayed nanobody facilitated a more targeted release of the toxin, resulting in the elimination of a significant portion of the *in vitro* spheroid mass. This novel system holds promise for effectively delivering therapeutic agents to tumor cells through specific binding, while mitigating adverse effects on healthy tissue.

The same experiment was repeated for triple-negative MDA-MB-231 cells. Confocal images (Figure 25) show little to no change in spheroid area for all four groups in this cell line. A stark difference is noticed between this set of images and those taken for JIMT1 spheroids.

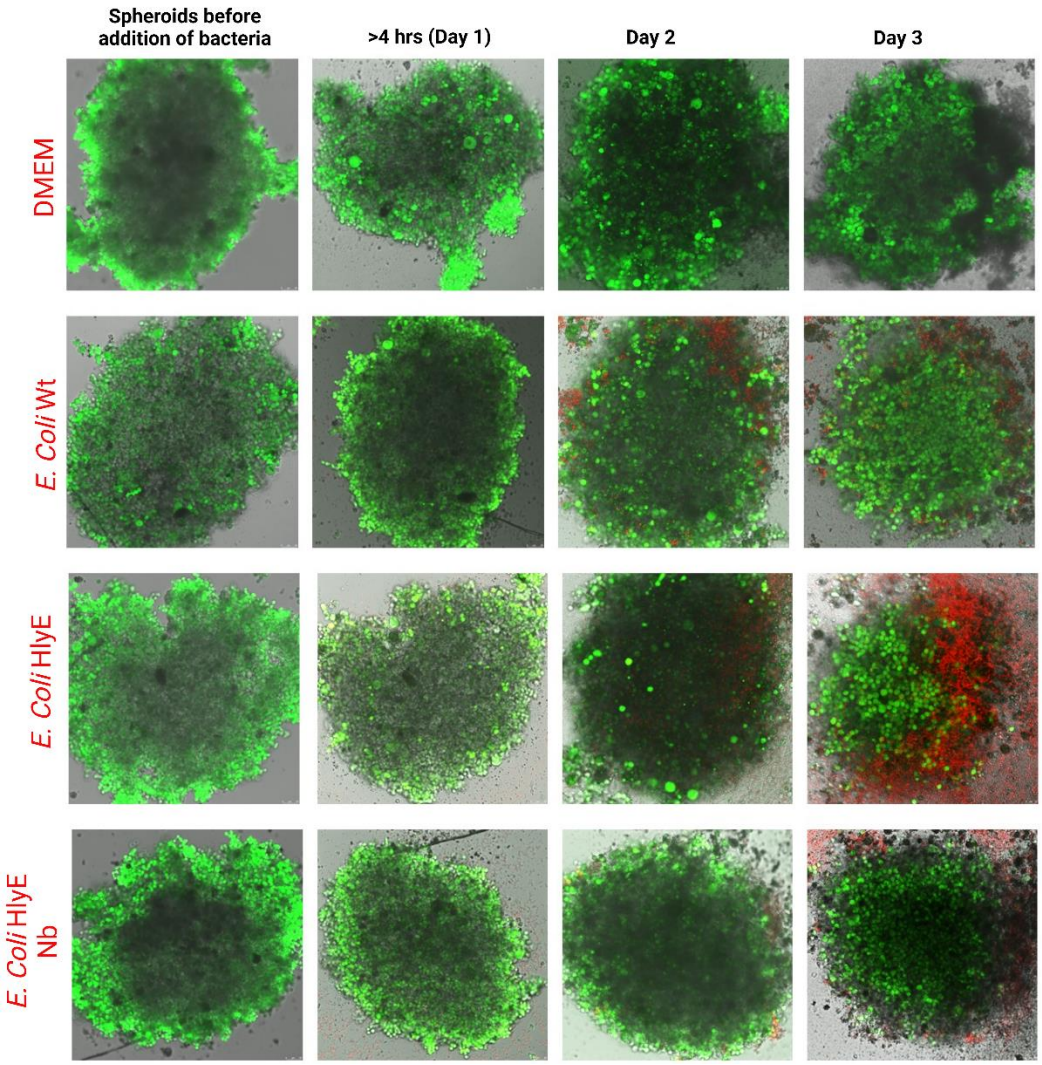

Figure 25: Confocal microscopy images of MDA-MB-231 spheroids experiment

3.4.2 Analysis of 3D Assay Results Using ImageJ Software

We conducted an analysis of four replicate sets of images for each day and experimental group using ImageJ software. In summary, the images underwent initial color threshold adjustments within the LAB setting after establishing a global scale. Subsequently, the 'Analyze Particles' option was employed to measure the spheroid area. The threshold was uniformly adjusted to eliminate noise based on standardized adjustments corresponding to image exposures. In instances where scattered cells were present on Day 3 in the *E. coli BL21* HlyE

and *E. coli BL21* HlyE Nb groups, the 'Despeckle' setting was fine-tuned to ensure precision. Following the determination of areas for each day, the results were normalized by calculating the percentage area relative to the initial spheroid area.

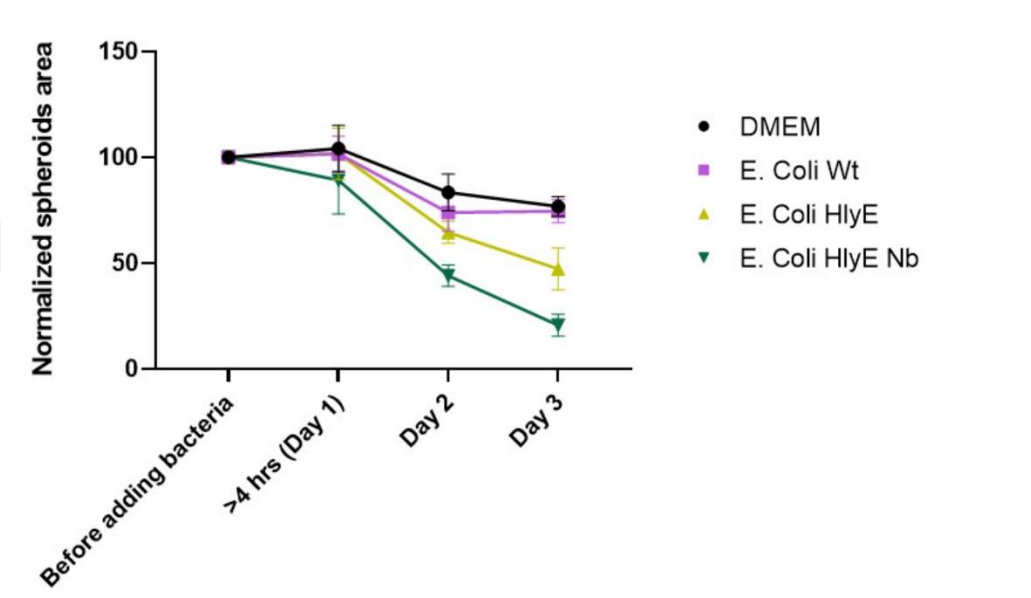

Figure 26: ImageJ analysis of JIMT1 spheroid images. The graph shows observed trend of spheroid area amongst four groups over the three-day period.

The outcomes from ImageJ analysis are visually depicted in Figure 26, revealing discernible trends across both days and groups. Figure 26 graphically illustrates that, four hours post-bacterial induction, the spheroid sizes exhibited relative stability. However, by Day 2, a more pronounced reduction in spheroid area became evident, with a significant decline observed in both the *E. coli BL21* HlyE and *E. coli BL21* HlyE Nb groups. Additionally, under control DMEM conditions, a progressive decline in spheroid area was noted by Day 3, mirroring the trend observed in the *E. coli BL21* group. A further and more pronounced

decrease in spheroid area was observed in the *E. coli BL21* HlyE and *E. coli BL21* HlyE Nb groups on Day 3. The most substantial reduction occurred in JIMT1 spheroids treated with *E. coli BL21* HlyE Nb on all four days. Statistical analyses, including ANOVA and multiple t-tests, are presented for verification of significance (Figures 27 A and B). Collectively, these results strongly indicate that the utilization of our genetically engineered bacteria, featuring both nanobody and toxin, had the most profound impact on JIMT1 cell spheroids compared to other experimental groups.

A)

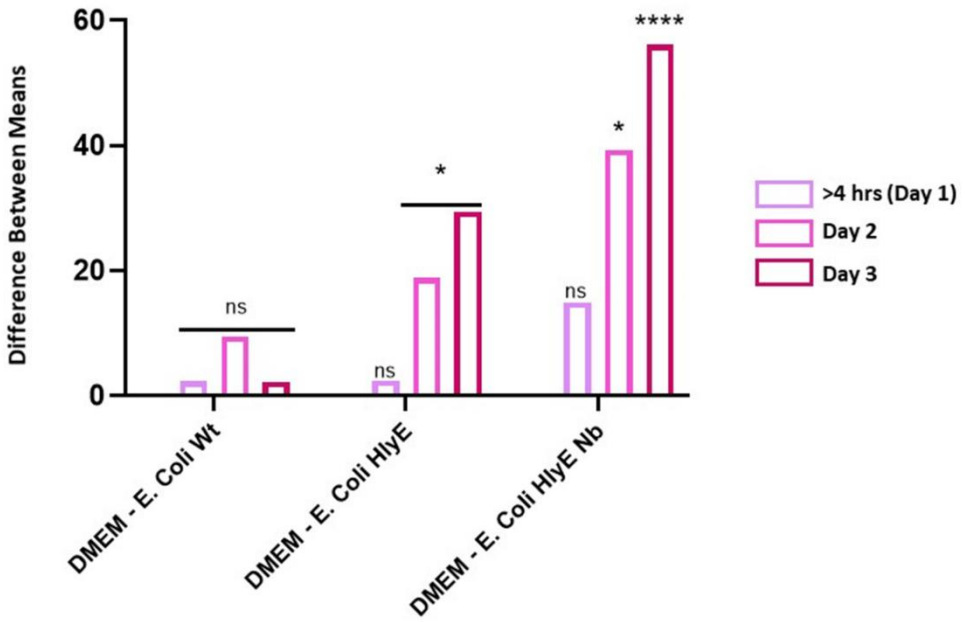
Difference Between Means
60
40
20
0
ns
*
ns
*
ns
****
DMEM - E. Coli Wt
DMEM - E. Coli HlyE
DMEM - E. Coli HlyE Nb
>4 hrs (Day 1)
Day 2
Day 3

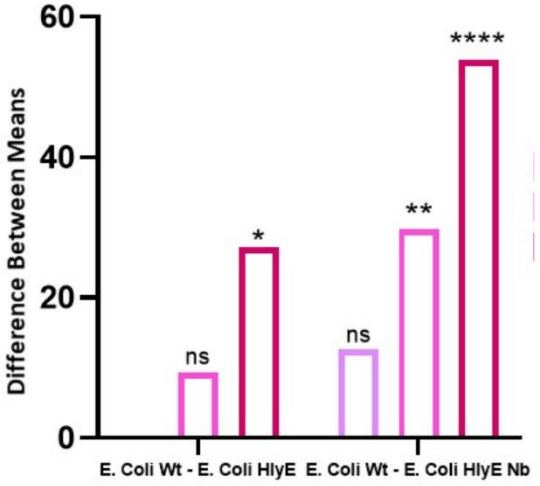
Difference Between Means
60
40
20
0
ns
*
ns
**
****
E. Coli Wt - E. Coli HlyE
E. Coli Wt - E. Coli HlyE Nb

B)

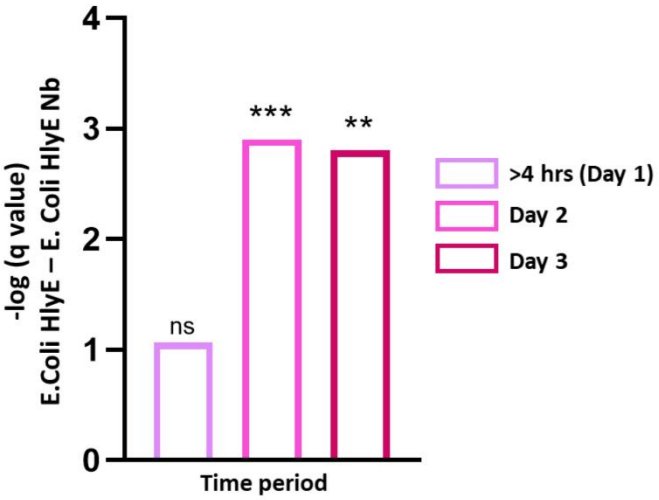
-log (q value)
E.Coli HlyE – E. Coli HlyE Nb
4
3
2
1
0
ns
***
**
Time period
>4 hrs (Day 1)
Day 2
Day 3

Figure 27: (A) Two-way ANOVA for comparison between groups with DMEM as control group in the first graph and *E. coli BL21* as control in the second graph. (B) Multiple t-test for comparison between groups *E. coli BL21* HlyE and *E. coli BL21* HlyE Nb.

The ANOVA graph with DMEM as control group shows no significant difference between DMEM group of JIMT1 cells and *E. coli BL21* group of JIMT1 cells over all three days. On day 2 a significant difference (*) is observed between DMEM group and both *E. coli BL21* HlyE and *E. coli BL21* HlyE Nb. On day 3 this difference remains the same between DMEM treated JIMT1 cells and those treated with *E. coli BL21* HlyE. However a much more pronounced and significant difference (****) is observed between control group and *E. coli BL21* HlyE Nb treated JIMT1 cells. Two-way ANOVA was also carried out with *E. coli BL21* as the control group. Difference in spheroid area is only significant (*) between *E. coli BL21* and *E. coli BL21* HlyE groups on day 3. A greater difference is shown between *E. coli BL21* and *E. coli BL21* HlyE Nb groups on day 2 (**) and day 3 (****). Multiple t-tests were also done to analyze the two groups *E. coli BL21* HlyE and *E. coli BL21* HlyE Nb and account for differences over the three-day experimental period. A significant difference both on day 2 (***) and day 3 (**) was observed indicating superiority of out proposed engineered design *E. coli BL21* HlyE Nb in targeted elimination of JIMT1 breast cancer cells.

3.4.3 CellTiter-Glo 3D Cell Viability Assay

The assessment of spheroid viability was conducted using the CellTiter-Glo 3D Cell Viability Assay, a luminescence-based method, and the outcomes are illustrated in Figures 28 and 29. Examining the fold-change values for JIMT1 and MDA-MB-231, a gradual and successive decline in cell viability was observed across the various experimental groups in both cell lines. Notably, a more pronounced decrease was evident in the JIMT1 dataset when considering the experimental groups (Figure 28 A).

The application of one-way ANOVA (Figure 28 B) to compare DMEM with other groups revealed no significant difference between DMEM and *E. coli BL21* in the case of JIMT1 cells. However, a noteworthy difference was identified between DMEM and both *E. coli BL21* HlyE (**), and *E. coli BL21* HlyE Nb (***). Further analysis, comparing group means with *E. coli BL21* as the reference (Figure 28 C), indicated a significant difference with *E. coli BL21* HlyE (**) and a highly significant difference with *E. coli BL21* HlyE Nb (***), the primary engineered bacterial strain. Additionally, a t-test between *E. coli BL21* HlyE and *E. coli BL21* HlyE Nb (Figure 29) revealed a significant difference (*), confirming the superior efficacy of *E. coli BL21* HlyE Nb in eradicating JIMT1 cell spheroids.

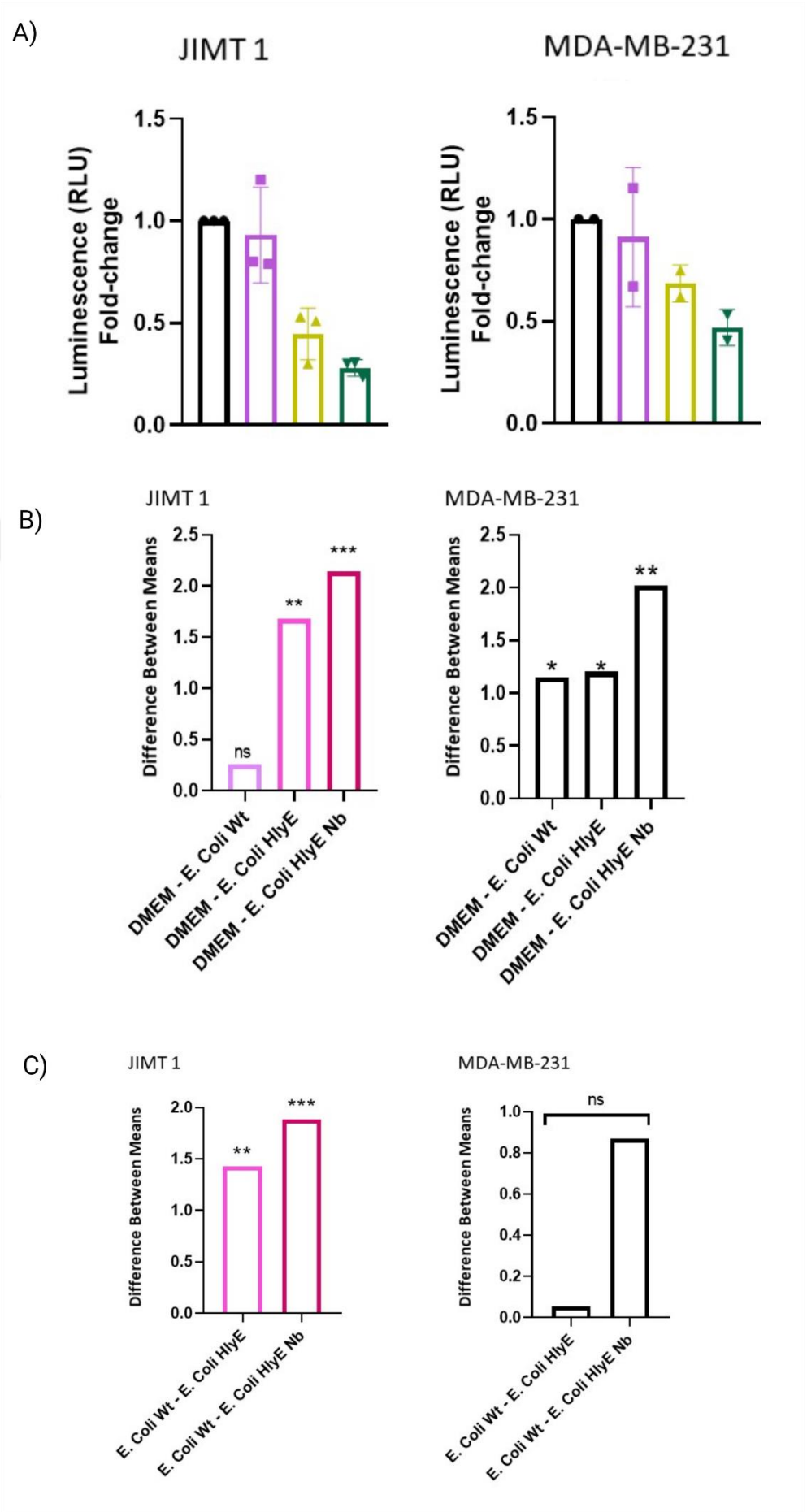
A)
JIMT 1
MDA-MB-231
Luminescence (RLU)
Fold-change
1.5
1.0
0.5
0.0
B)
JIMT 1
MDA-MB-231
Difference Between Means
2.5
2.0
1.5
1.0
0.5
0.0
ns
**
***
*
*
**
DMEM - E. Coli Wt
DMEM - E. Coli HlyE
DMEM - E. Coli HlyE Nb
C)
JIMT 1
MDA-MB-231
Difference Between Means
2.0
1.5
1.0
0.5
0.0
**
***
ns
1.0
0.8
0.6
0.4
0.2
0.0
E. Coli Wt - E. Coli HlyE
E. Coli Wt - E. Coli HlyE Nb

Figure 28: CellTiter-Glo 3D Cell Viability Assay graphs (A) Normalized fold-change luminescence data for JIMT1 and MDA-MB-231 (B) One-way ANOVA with DMEM as control group (C) One-way ANOVA with *E. coli BL21* as control group

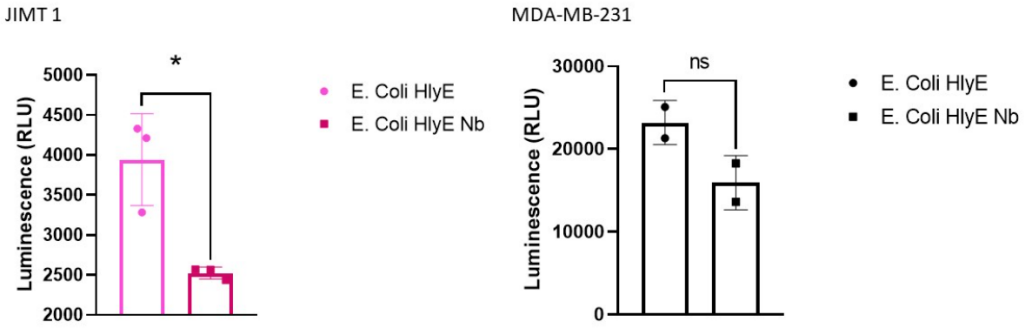

Figure 29: t-test between *E. coli BL21* HlyE and *E. coli BL21* HlyE Nb for JIMT1 and MDA-MB-231 cells.

In contrast, analysis of the triple-negative MDA-MB-231 control cell line demonstrated a decline in cell viability across the groups. However, the one-way ANOVA (Figure 28 C), utilizing *E. coli BL21* as the control, did not reveal significant differences with both *E. coli BL21* HlyE and *E. coli BL21* HlyE Nb. Similarly, a t-test comparing differences between the *E. coli BL21* HlyE and *E. coli BL21* HlyE Nb groups (Figure 29) showed no significance. These results align with expectations, as the engineered bacterial system is designed to specifically target HER2 receptors, demonstrating efficacy against JIMT1 cells while exhibiting reduced effectiveness against triple-negative MDA-MB-231 cells.

CHAPTER IV: CONCLUSION

Recent preclinical investigations highlight the efficacy of bacteria-based therapeutics in addressing drug-resistant tumors, notorious for their resistance to traditional treatments. These therapies, by selectively targeting cancer cells and minimizing harm to healthy cells, hold the potential to significantly reduce common side effects associated with standard cancer treatments. Their ability to penetrate deep into tumor tissues, often unreachable by conventional methods, provides a distinct advantage. Despite existing challenges in clinical application, cutting-edge research is progressing to refine bacteria-based therapies for the future of cancer treatment. Advances in genetic engineering and biotechnology are paving the way for more sophisticated therapies, engineered to produce therapeutic agents like cytokines and checkpoint inhibitors, enhancing the body's immune response against cancer. Combination therapies, integrating bacteria-based approaches with radiation and immunotherapy, are being explored to improve cancer treatment efficacy. Notably, there's potential for bacteria-based therapies to deliver targeted treatments to the brain, overcoming limitations imposed by the blood-brain barrier.

In our research, we explored the fusion of bacteria-based therapeutics with nanotechnology for precise toxin delivery. Utilizing a biological nanobody (Nb), we facilitated the attachment of engineered *E. coli* to JIMT1 breast cancer cells, designed to release the HlyE toxin, directly targeting cancer cells. Our engineered *E. coli* strain, *E. coli BL21* HlyE Nb, displayed Nb specific to HER2 receptors, commonly overexpressed in breast cancer cells, yielding positive results in both 2D and 3D assays. Our adaptable methodology holds promise for various cancer

types, offering a proof of concept for bacteria-based therapeutics combined with nanotechnology in targeted cancer treatment. Envisioning our work as a catalyst for further research, we anticipate refining therapeutic strategies for future applications.

Looking ahead, the potential of bacteria-based therapy in cancer treatment is highly encouraging, supported by ongoing advancements in synthetic biology, genetic engineering, biotechnology, and drug delivery systems. Bacteria's modifiability and cost-effective production make them an attractive therapeutic option, diversifying treatments and improving outcomes for cancer patients. The future of cancer therapy appears promising through the continued exploration and translation of bacteria-based therapies into practical solutions for patients.

BIBLIOGRAPHY

[1] S. Sharma, T. K. Kelly, and P. A. Jones, “Epigenetics in cancer,” *Carcinogenesis*, vol. 31, no. 1, pp. 27–36, Jan. 2010, doi: 10.1093/carcin/bgp220.

[2] L. Gattinoni, D. J. Powell, S. A. Rosenberg, and N. P. Restifo, “Adoptive immunotherapy for cancer: building on success,” *Nat. Rev. Immunol.*, vol. 6, no. 5, Art. no. 5, May 2006, doi: 10.1038/nri1842.

[3] L. M. Weiner, J. C. Murray, and C. W. Shuptrine, “Antibody-Based Immunotherapy of Cancer,” *Cell*, vol. 148, no. 6, pp. 1081–1084, Mar. 2012, doi: 10.1016/j.cell.2012.02.034.

[4] “Biomolecules | Free Full-Text | Nano-Based Approved Pharmaceuticals for Cancer Treatment: Present and Future Challenges.” Accessed: Dec. 13, 2023. [Online]. Available: https://www.mdpi.com/2218-273X/12/6/784

[5] K. Park, “Facing the Truth about Nanotechnology in Drug Delivery,” *ACS Nano*, vol. 7, no. 9, pp. 7442–7447, Sep. 2013, doi: 10.1021/nn404501g.

[6] S. Shukla and A. Mehta, “Anticancer potential of medicinal plants and their phytochemicals: a review,” *Braz. J. Bot.*, vol. 38, no. 2, pp. 199–210, Jun. 2015, doi: 10.1007/s40415-015-0135-0.

[7] K. Fiedler, S. Lazzaro, J. Lutz, S. Rauch, and R. Heidenreich, “mRNA Cancer Vaccines,” in *Current Strategies in Cancer Gene Therapy*, W. Walther, Ed., in Recent Results in Cancer Research. , Cham: Springer International Publishing, 2016, pp. 61–85. doi: 10.1007/978-3-319-42934-2_5.

[8] L. Miao, Y. Zhang, and L. Huang, “mRNA vaccine for cancer immunotherapy,” *Mol. Cancer*, vol. 20, no. 1, p. 41, Feb. 2021, doi: 10.1186/s12943-021-01335-5.

[9] R. Jia *et al.*, “Advances in Multiple Stimuli-Responsive Drug-Delivery Systems for Cancer Therapy,” *Int. J. Nanomedicine*, vol. 16, pp. 1525–1551, Feb. 2021, doi:

10.2147/IJN.S293427.

[10] M. T.-Q. Duong, Y. Qin, S.-H. You, and J.-J. Min, “Bacteria-cancer interactions: bacteria-based cancer therapy,” *Exp. Mol. Med.*, vol. 51, no. 12, Art. no. 12, Dec. 2019, doi: 10.1038/s12276-019-0297-0.

[11] K. S. Allemailem, “Innovative Approaches of Engineering Tumor-Targeting Bacteria with Different Therapeutic Payloads to Fight Cancer: A Smart Strategy of Disease Management,” *Int. J. Nanomedicine*, vol. 16, pp. 8159–8184, Dec. 2021, doi: 10.2147/IJN.S338272.

[12] T. Chien, A. Doshi, and T. Danino, “Advances in bacterial cancer therapies using synthetic biology,” *Curr. Opin. Syst. Biol.*, vol. 5, pp. 1–8, Oct. 2017, doi: 10.1016/j.coisb.2017.05.009.

[13] J. Lee, A. C. Keates, and C. J. Li, “Synthetic Biology Medicine and Bacteria-Based Cancer Therapeutics,” *Methods Mol. Biol. Clifton NJ*, vol. 2323, pp. 267–280, 2021, doi: 10.1007/978-1-0716-1499-0_19.

[14] S. Chowdhury, S. Castro, C. Coker, T. E. Hinchliffe, N. Arpaia, and T. Danino, “Programmable bacteria induce durable tumor regression and systemic antitumor immunity,” *Nat. Med.*, vol. 25, no. 7, pp. 1057–1063, Jul. 2019, doi: 10.1038/s41591-019-0498-z.

[15] R. M. Shih and Y. Y. Chen, “Engineering Principles for Synthetic Biology Circuits in Cancer Immunotherapy,” *Cancer Immunol. Res.*, vol. 10, no. 1, pp. 6–11, Jan. 2022, doi: 10.1158/2326-6066.CIR-21-0769.

[16] M.-R. Wu, B. Jusiak, and T. K. Lu, “Engineering advanced cancer therapies with synthetic biology,” *Nat. Rev. Cancer*, vol. 19, no. 4, pp. 187–195, Apr. 2019, doi: 10.1038/s41568-019-0121-0.

[17] J. O. e S. F. Brandão, “Streptococcus pyogenes in tumor treatment: the past,

present and future," Jun. 2020, Accessed: Dec. 16, 2023. [Online]. Available: https://repositorio-aberto.up.pt/handle/10216/128759

[18] W. B. Coley, "The treatment of malignant tumors by repeated inoculations of erysipelas. With a report of ten original cases. 1893," *Clin. Orthop.*, no. 262, pp. 3–11, Jan. 1991.

[19] R. D. Carlson, J. C. Flickinger, and A. E. Snook, "Talkin' Toxins: From Coley's to Modern Cancer Immunotherapy," *Toxins*, vol. 12, no. 4, p. 241, Apr. 2020, doi: 10.3390/toxins12040241.

[20] S. Senapati, A. K. Mahanta, S. Kumar, and P. Maiti, "Controlled drug delivery vehicles for cancer treatment and their performance," *Signal Transduct. Target. Ther.*, vol. 3, no. 1, Art. no. 1, Mar. 2018, doi: 10.1038/s41392-017-0004-3.

[21] T. Danino, A. Prindle, J. Hasty, and S. Bhatia, "Measuring growth and gene expression dynamics of tumor-targeted S. typhimurium bacteria," *J. Vis. Exp. JoVE*, no. 77, p. e50540, Jul. 2013, doi: 10.3791/50540.

[22] J. C. Anderson, E. J. Clarke, A. P. Arkin, and C. A. Voigt, "Environmentally controlled invasion of cancer cells by engineered bacteria," *J. Mol. Biol.*, vol. 355, no. 4, pp. 619–627, Jan. 2006, doi: 10.1016/j.jmb.2005.10.076.

[23] J. R. Cubillos-Ruiz and A. Cubillos-Ruiz, "Engineered bacteria recycle tumor metabolic waste to boost immunotherapy," *Cell Host Microbe*, vol. 29, no. 12, pp. 1725–1727, Dec. 2021, doi: 10.1016/j.chom.2021.11.008.

[24] Z. Hosseinidoust, B. Mostaghaci, O. Yasa, B.-W. Park, A. V. Singh, and M. Sitti, "Bioengineered and biohybrid bacteria-based systems for drug delivery," *Adv. Drug Deliv. Rev.*, vol. 106, no. Pt A, pp. 27–44, Nov. 2016, doi: 10.1016/j.addr.2016.09.007.

[25] S. Soleimanpour, S. M. Hasanian, A. Avan, A. Yaghoubi, and M. Khazaei,

"Bacteriotherapy in gastrointestinal cancer," *Life Sci.*, vol. 254, p. 117754, Aug. 2020, doi: 10.1016/j.lfs.2020.117754.

[26] R. Raj and S. Das, "Prospects of Bacteriotherapy with Nanotechnology in Nanoparticledrug Conjugation Approach for Cancer Therapy," *Curr. Med. Chem.*, vol. 23, no. 14, pp. 1477–1494, 2016, doi: 10.2174/0929867323666160406120923.

[27] V. H. Nguyen and J.-J. Min, "Salmonella-Mediated Cancer Therapy: Roles and Potential," *Nucl. Med. Mol. Imaging*, vol. 51, no. 2, pp. 118–126, Jun. 2017, doi: 10.1007/s13139-016-0415-z.

[28] M. Yavuz, M. Ütkür, E. Ş. Kehribar, E. Yağız, E. Ü. Sarıtaş, and U. Ö. Ş. Şeker, "Engineered Bacteria with Genetic Circuits Accumulating Nanomagnets as MRI Contrast Agents," *Small Weinh. Bergstr. Ger.*, vol. 18, no. 26, p. e2200537, Jul. 2022, doi: 10.1002/smll.202200537.

[29] T. Danino, J. Lo, A. Prindle, J. Hasty, and S. N. Bhatia, "In Vivo Gene Expression Dynamics of Tumor-Targeted Bacteria," *ACS Synth. Biol.*, vol. 1, no. 10, pp. 465–470, Oct. 2012, doi: 10.1021/sb3000639.

[30] V. Raman *et al.*, "Intracellular delivery of protein drugs with an autonomously lysing bacterial system reduces tumor growth and metastases," *Nat. Commun.*, vol. 12, no. 1, p. 6116, Oct. 2021, doi: 10.1038/s41467-021-26367-9.

[31] N. Elliott, T. Lee, L. You, and F. Yuan, "Proliferation behavior of E. coli in a three-dimensional in vitro tumor model," *Integr. Biol. Quant. Biosci. Nano Macro*, vol. 3, no. 6, pp. 696–705, Jun. 2011, doi: 10.1039/c0ib00137f.

[32] T. Harimoto *et al.*, "Rapid screening of engineered microbial therapies in a 3D multicellular model," *Proc. Natl. Acad. Sci. U. S. A.*, vol. 116, no. 18, pp. 9002–9007, Apr. 2019, doi: 10.1073/pnas.1820824116.

[33] M. Xie and M. Fussenegger, "Designing cell function: assembly of synthetic

gene circuits for cell biology applications," *Nat. Rev. Mol. Cell Biol.*, vol. 19, no. 8, Art. no. 8, Aug. 2018, doi: 10.1038/s41580-018-0024-z.

[34] T. K. Lu, A. S. Khalil, and J. J. Collins, "Next-generation synthetic gene networks," *Nat. Biotechnol.*, vol. 27, no. 12, Art. no. 12, Dec. 2009, doi: 10.1038/nbt.1591.

[35] T.-C. Tang *et al.*, "Materials design by synthetic biology," *Nat. Rev. Mater.*, vol. 6, no. 4, Art. no. 4, Apr. 2021, doi: 10.1038/s41578-020-00265-w.

[36] P.-F. Xia, H. Ling, J. L. Foo, and M. W. Chang, "Synthetic genetic circuits for programmable biological functionalities," *Biotechnol. Adv.*, vol. 37, no. 6, p. 107393, Nov. 2019, doi: 10.1016/j.biotechadv.2019.04.015.

[37] I. C. MacDonald and T. L. Deans, "Tools and applications in synthetic biology," *Adv. Drug Deliv. Rev.*, vol. 105, pp. 20–34, Oct. 2016, doi: 10.1016/j.addr.2016.08.008.

[38] Y. Higashikuni, W. C. Chen, and T. K. Lu, "Advancing therapeutic applications of synthetic gene circuits," *Curr. Opin. Biotechnol.*, vol. 47, pp. 133–141, Oct. 2017, doi: 10.1016/j.copbio.2017.06.011.

[39] R. W. Bradley, M. Buck, and B. Wang, "Tools and Principles for Microbial Gene Circuit Engineering," *J. Mol. Biol.*, vol. 428, no. 5, Part B, pp. 862–888, Feb. 2016, doi: 10.1016/j.jmb.2015.10.004.

[40] Q. Liu, J. Schumacher, X. Wan, C. Lou, and B. Wang, "Orthogonality and Burdens of Heterologous AND Gate Gene Circuits in E. coli," *ACS Synth. Biol.*, vol. 7, no. 2, pp. 553–564, Feb. 2018, doi: 10.1021/acssynbio.7b00328.

[41] J. Shin and V. Noireaux, "An E. coli Cell-Free Expression Toolbox: Application to Synthetic Gene Circuits and Artificial Cells," *ACS Synth. Biol.*, vol. 1, no. 1, pp. 29–41, Jan. 2012, doi: 10.1021/sb200016s.

[42] B. Jusiak, S. Cleto, P. Perez-Piñera, and T. K. Lu, "Engineering Synthetic Gene

Circuits in Living Cells with CRISPR Technology," *Trends Biotechnol.*, vol. 34, no. 7, pp. 535–547, Jul. 2016, doi: 10.1016/j.tibtech.2015.12.014.

[43] L. T. Bereza-Malcolm, G. Mann, and A. E. Franks, "Environmental Sensing of Heavy Metals Through Whole Cell Microbial Biosensors: A Synthetic Biology Approach," *ACS Synth. Biol.*, vol. 4, no. 5, pp. 535–546, May 2015, doi: 10.1021/sb500286r.

[44] B. Wang, M. Barahona, and M. Buck, "A modular cell-based biosensor using engineered genetic logic circuits to detect and integrate multiple environmental signals," *Biosens. Bioelectron.*, vol. 40, no. 1, pp. 368–376, Feb. 2013, doi: 10.1016/j.bios.2012.08.011.

[45] S. Kannappan and B. C. M. Ramisetty, "Engineered Whole-Cell-Based Biosensors: Sensing Environmental Heavy Metal Pollutants in Water—a Review," *Appl. Biochem. Biotechnol.*, vol. 194, no. 4, pp. 1814–1840, Apr. 2022, doi: 10.1007/s12010-021-03734-2.

[46] G. B. Shahid, R. E. Ahan, J. Ostaku, and U. O. S. Seker, "A Bacterial Living Therapeutics with Engineered Protein Secretion Circuits To Eliminate Breast Cancer Cells." bioRxiv, p. 2023.04.27.538589, Apr. 27, 2023. doi: 10.1101/2023.04.27.538589.

[47] R. E. Ahan, B. M. Kırpat, B. Saltepe, and U. Ö. Ş. Şeker, "A Self-Actuated Cellular Protein Delivery Machine," *ACS Synth. Biol.*, vol. 8, no. 4, pp. 686–696, Apr. 2019, doi: 10.1021/acssynbio.9b00062.

[48] B. M. Kırpat Konak, M. E. Bakar, R. E. Ahan, E. U. Özyürek, S. Dökmeci, and U. Ö. Şafak Şeker, "A living material platform for the biomineralization of biosilica," *Mater. Today Bio*, vol. 17, p. 100461, Dec. 2022, doi: 10.1016/j.mtbio.2022.100461.

[49] M. Pruszynski *et al.*, "The Therapeutic Potential of Anti-HER2 2Rs15d

Nanobody Labeled with 225Ac – an In Vitro and In Vivo Evaluation," *J. Med. Imaging Radiat. Sci.*, vol. 50, no. 1, p. S7, Mar. 2019, doi: 10.1016/j.jmir.2019.03.023.

[50] G. Zhang, S. Brokx, and J. H. Weiner, "Extracellular accumulation of recombinant proteins fused to the carrier protein YebF in Escherichia coli," *Nat. Biotechnol.*, vol. 24, no. 1, pp. 100–104, Jan. 2006, doi: 10.1038/nbt1174.

[51] K. Rennstam *et al.*, "Cytogenetic characterization and gene expression profiling of the trastuzumab-resistant breast cancer cell line JIMT-1," *Cancer Genet. Cytogenet.*, vol. 172, no. 2, pp. 95–106, Jan. 2007, doi: 10.1016/j.cancergencyto.2006.09.014.

[52] K. Subik *et al.*, "The Expression Patterns of ER, PR, HER2, CK5/6, EGFR, Ki-67 and AR by Immunohistochemical Analysis in Breast Cancer Cell Lines," *Breast Cancer*, vol. 4, pp. 35–41, May 2010.

[53] T. Harimoto, D. Deb, and T. Danino, "A rapid screening platform to coculture bacteria within tumor spheroids," *Nat. Protoc.*, vol. 17, no. 10, pp. 2216–2239, Oct. 2022, doi: 10.1038/s41596-022-00723-5.

APPENDIX A

DNA SEQUENCES OF CONSTRUCTS

Table A 1: DNA Sequences used in this study

Name	Type	Sequence 5'-to-3'
2Rs15D	Nanobody	CAGGTGCAGCTGCAGGAAAGCGGCGGCG GCAGCGTGCAGGCGGGCGGCAGCCTGAA ACTGACCTGCGCGGCGAGCGGCTATATTT TTAACAGCTGCGGCATGGGCTGGTATCGC CAGAGCCCGGGCCGCGAACGCGAACTGG TGAGCCGCATTAGCGGCGATGGCGATACC TGGCATAAAGAAAGCGTGAAAGGCCGCTT TACCATTAGCCAGGATAACGTGAAAAAAAC CCTGTATCTGCAGATGAACAGCCTGAAAC CGGAAGATACCGCGGTGTATTTTTGCGCG GTGTGCTATAACCTGGAAACCTATTGGGG CCAGGGCACCCAGGTGACCGTGAGCAGC
2Rs15D ordered fragement	Nanobody	GCCCAGCCGGCGATGGCCATGGGCACTA GTCAGGTGCAGCTGCAGGAAAGCGGCGG CGGCAGCGTGCAGGCGGGCGGCAGCCTG AAACTGACCTGCGCGGCGAGCGGCTATAT TTTTAACAGCTGCGGCATGGGCTGGTATC GCCAGAGCCCGGGCCGCGAACGCGAACT GGTGAGCCGCATTAGCGGCGATGGCGAT ACCTGGCATAAAGAAAGCGTGAAAGGCCG CTTTACCATTAGCCAGGATAACGTGAAAAA AACCCTGTATCTGCAGATGAACAGCCTGA AACCGGAAGATACCGCGGTGTATTTTTGC GCGGTGTGCTATAACCTGGAAACCTATTG GGGCCAGGGCACCCAGGTGACCGTGAGC AGCCTTAAGCGCACAACCATCAATAAAAAC GGT
pelB	Signal sequence	ATGAAATACCTGCTGCCGACCGCTGCTGC TGGTCTGCTGCTCCTCGCTGCCCAGCCGG CGATGGCC
Ag43 (160 N alpha subunit)	Autotransporter Protein	CGCACAACCATCAATAAAAACGGTCGCCA GATTGTGAGAGCTGAAGGAACGGCAAATA CCACTGTGGTTTATGCCGGCGGCGACCAG ACTGTACATGGTCACGCACTGGATACCAC GCTGAATGGGGGATACCAGTATGTGCACA ACGGCGGTACAGCGTCTGACACTGTTGTG AACAGTGACGGCTGGCAGATTGTCAAAAA CGGGGGTGTGGCCGGGAATACCACCGTT AATCAGAAGGGCAGACTGCAGGTGGACG

		CCGGTGGTACAGCCACGAATGTCACCCTG AAGCAGGGCGGCGCACTGGTTACCAGTAC GGCTGCAACCGTTACCGGCATAAACCGCC TGGGAGCATTCTCTGTTGTGGAGGGTAAA GCTGATAATGTCGTACTGGAAAATGGCGG ACGCCTGGATGTGCTGACCGGACACACAG CCACTAATACCCGCGTGGATGATGGCGGA ACGCTGGATGTCCGCAACGGTGGCACCG CCACCACCGTATCCATGGGAAATGGCGGT GTACTGCTGGCCGATTCCGGTGCCGCTGT CAGTGGTACCCGGAGCGACGGAAAGGCA TTCAGTATCGGAGGCGGTCAGGCGGATGC CCTGATGCTGGAAAAAGGCAGTTCATTCA CGCTGAACGCCGGTGATACGGCCACGGA TACCACGGTAAATGGCGGACTGTTCACCG CCAGGGGCGGCACACTGGCGGGCACCAC CACGCTGAATAACGGCGCCATACTTACCC TTTCCGGGAAGACGGTGAACAACGATACC CTGACCATCCGTGAAGGCGATGCACTCCT GCAGGGAGGCTCTCTCACCGGTAACGGC AGCGTGGAAAAATCAGGAAGTGGCACACT CACTGTCAGCAACACCACACTCACCCAGA AAGCCGTCAACCTGAATGAAGGCACGCTG ACGCTGAACGACAGTACCGTCACCACGGA TGTCATTGCTCAGCGCGGTACAGCCCTGA AGCTGACCGGCAGCACTGTGCTGAACGGT GCCATTGAC
Ag43 (Beta subunit)	Autotransporter protein	CCCACGAATGTCACTCTCGCCTCCGGTGC CACCTGGAATATCCCCGATAACGCCACGG TGCAGTCGGTGGTGGATGACCTCAGCCAT GCCGGACAGATTCATTTCACCTCCACCCG CACAGGGAAGTTCGTACCGGCAACCCTGA AAGTGAAAAACCTGAACGGACAGAATGGC ACCATCAGCCTGCGTGTACGCCCGGATAT GGCACAGAACAATGCTGACAGACTGGTCA TTGACGGCGGCAGGGCAACCGGAAAAAC CATCCTGAACCTGGTGAACGCCGGCAACA GTGCGTCGGGGCTGGCGACCAGCGGTAA GGGTATTCAGGTGGTGGAAGCCATTAACG GTGCCACCACGGAGGAAGGGGCCTTTGT CCAGGGGAACAGGCTGCAGGCCGGTGCC TTTAACTACTCCCTCAACCGGGACAGTGAT GAGAGCTGGTATCTGCGCAGTGAAAATGC TTATCGTGCAGAAGTCCCCCTGTATGCCT CCATGCTGACACAGGCAATGGACTATGAC CGGATTGTGGCAGGCTCCCGCAGCCATCA GACCGGTGTAAATGGTGAAAACAACAGCG TCCGTCTCAGCATTCAGGGCGGTCATCTC GGTCACGATAACAATGGCGGTATTGCCCG TGGGGCCACGCCGGAAAGCAGCGGCAGC TATGGATTC GTCCGTCTGGAGGGTGACCTGATGAGAAC AGAGGTTGCCGGTATGTCTGTGACCGCGG

		GGGTATATGGTGCTGCTGGCCATTCTTCC GTTGATGTTAAGGATGATGACGGCTCCCG TGCCGGCACGGTCCGGGATGATGCCGGC AGCCTGGGCGGATACCTGAATCTGGTACA CACGTCCTCCGGCCTGTGGGCTGACATTG TGGCACAGGGAACCCGCCACAGCATGAAA GCGTCATCGGACAATAACGACTTCCGCGC CCGGGGCTGGGGCTGGCTGGGCTCACTG GAAACCGGTCTGCCCTTCAGTATCACTGA CAACCTGATGCTGGAGCCACAACTGCAGT ATACCTGGCAGGGACTTTCCCTGGATGAC GGTAAGGACAACGCCGGTTATGTGAAGTT CGGGCATGGCAGTGCACAACATGTGCGTG CCGGTTTCCGTCTGGGCAGCCACAACGAT ATGACCTTTGGCGAAGGCACCTCATCCCG TGCCCCCCTGCGTGACAGTGCAAAACACA GTGTGAGTGAATTACCGGTGAACTGGTGG GTACAGCCTTCTGTTATCCGCACCTTCAGC TCCCGGGGAGATATGCGTGTGGGGACTTC CACTGCAGGCAGCGGGATGACGTTCTCTC CCTCACAGAATGGCACATCACTGGACCTG CAGGCCGGACTGGAAGCCCGTGTCCGGG AAAATATCACCCTGGGCGTTCAGGCCGGT TATGCCCACAGCGTCAGCGGCAGCAGCG CTGAAGGGTATAACGGTCAGGCCACACTG AATGTGACCTTC
HlyE	Pore-forming Toxin	ATGACTGAAATCGTTGCAGATAAAACGGTA GAAGTAGTTAAAAACGCAATCGAAACCGC AGATGGAGCATTAGATCTTTATAATAAATA TCTCGATCAGGTCATCCCCTGGCAGACCT TTGATGAAACCATAAAAGAGTTAAGTCGCT TTAAACAGGAGTATTCACAGGCAGCCTCC GTTTTAGTCGGCGATATTAAAACCTTACTT ATGGATAGCCAGGATAAGTATTTTGAAGCA ACCCAAACAGTGTATGAATGGTGTGGTGT TGCGACGCAATTGCTCGCAGCGTATATTTT GCTATTTGATGAGTACAATGAGAAGAAAGC ATCCGCCCAGAAAGACATTCTCATTAAGGT ACTGGATGACGGCATCACGAAGCTGAATG AAGCGCAAAAATCCCTGCTGGTAAGCTCA CAAAGTTTCAACAACGCTTCCGGGAAACT GCTGGCGTTAGATAGCCAGTTAACCAATG ATTTTTCAGAAAAAAGCAGCTATTTCCAGT CACAGGTAGATAAAATCAGGAAGGAAGCA TATGCCGGTGCCGCAGCCGGTGTCGTCG CCGGTCCATTTGGATTAATCATTTCCTATT CTATTGCTGCGGGCGTAGTTGAAGGAAAA CTGATTCCAGAATTGAAGAACAAGTTAAAA TCTGTGCAGAATTTCTTTACCACCCTGTCT AACACGGTTAAACAAGCGAATAAAGATATC GATGCCGCCAAATTGAAATTAACCACCGA AATAGCCGCCATCGGTGAGATAAAAACGG AAACTGAAACAACCAGATTCTACGTTGATT ATGATGATTTAATGCTTTCTTTGCTAAAAGA

		AGCGGCCAAAAAAATGATTAACACCTGTAA TGAGTATCAGAAAAGACACGGTAAAAAGA CACTCTTTGAGGTACCTGAAGTC
YebF	Secretion system	ATGAAAAAAAGAGGGGCGTTTTTAGGGCT GTTGTTGGTTTCTGCCTGCGCATCAGTTTT CGCTGCCAATAATGAAACCAGCAAGTCGG TCACTTTCCCAAAGTGTGAAGATCTGGATG CTGCCGGAATTGCCGCGAGCGTAAAACGT GATTATCAACAAAATCGCGTGGCGCGTTG GGCAGATGATCAAAAAATTGTCGGTCAGG CCGATCCCGTGGCTTGGGTCAGTTTGCAG GACATTCAGGGTAAAGATGATAAATGGTCA GTACCGCTAACCGTGCGTGGTAAAAGTGC CGATATTCATTACCAGGTCAGCGTGGACT GCAAAGCGGGAATGGCGGAATATCAGCG GCGT
Sec	Signal peptide	ATGAAAAAAAGAGGGGCGTTTTTAGGGCT GTTGTTGGTTTCTGCCTGCGCATCAGTTTT CGCT
T7 promoter	Promoter	TAATACGACTCACTATAGG
LacO	Promoter	GGAATTGTGAGCGGATAACAATTCC
T7 terminator	Terminator	CTAGCATAACCCCTTGGGGCCTCTAAACG GGTCTTGAGGGGTTTTTTG
rrnB T1	Terminator	CAAATAAAACGAAAGGCTCAGTCGAAAGA CTGGGCCTTTCGTTTTATCTGTTGTTTGTC GGTGAACGCTCTCCTGAGTAGGACAAAT
PL-TetO	Promoter	TCCCTATCAGTGATAGAGATTGACATCCCT ATCAGTGATAGAGATACTGAGCACATCAG CAGGACGCACTGACC
GST tag	Protein	ATGTCCCCTATACTAGGTTATTGGAAAATT AAGGGCCTTGTGCAACCCACTCGACTTCT TTTGGAATATCTTGAAGAAAAATATGAAGA GCATTTGTATGAGCGCGATGAAGGTGATA AATGGCGAAACAAAAAGTTTGAATTGGGTT TGGAGTTTCCCAATCTTCCTTATTATATTGA TGGTGATGTTAAATTAACACAGTCTATGGC CATCATACGTTATATAGCTGACAAGCACAA CATGTTGGGTGGTTGTCCAAAAGAGCGTG CAGAGATTTCAATGCTTGAAGGAGCGGTT TTGGATATTAGATACGGTGTTTCGAGAATT GCATATAGTAAAGACTTTGAAACTCTCAAA GTTGATTTTCTTAGCAAGCTACCTGAAATG CTGAAAATGTTCGAAGATCGTTTATGTCAT AAAACATATTTAAATGGTGATCATGTAACC CATCCTGACTTCATGTTGTATGACGCTCTT GATGTTGTTTTATACATGGACCCAATGTGC

		CTGGATGCGTTCCCAAAATTAGTTTGTTTT AAAAAACGTATTGAAGCTATCCCACAAATT GATAAGTACTTGAAATCCAGCAAGTATATA GCATGGCCTTTGCAGGGCTGGCAAGCCAC GTTTGGTGGTGGCGACCATCCTCCAAAA
mScarlet	Fluorescent protein	ATGAGTAAAGGAGAAGCTGTGATTAAAGA GTTCATGCGCTTCAAAGTTCACATGGAGGG TTCTATGAACGGTCACGAGTTCGAGATCGA AGGCGAAGGCGAGGGCCGTCCGTATGAAG GCACCCAGACCGCCAAACTGAAAGTGACT AAAGGCGGCCCGCTGCCTTTTTCCTGGGAC ATCCTGAGCCCGCAATTTATGTACGGTTCT AGGGCGTTCACCAAACACCCAGCGGATATC CCGGACTATTATAAGCAGTCTTTTCCGGAA GGTTTCAAGTGGGAACGCGTAATGAATTTT GAAGATGGTGGTGCCGTGACCGTCACTCAG GACACCTCCCTGGAGGATGGCACCCTGATC TATAAAGTTAAACTGCGTGGTACTAATTTT CCACCTGATGGCCCGGTGATGCAGAAAAA GACGATGGGTTGGGAGGCGTCTACCGAAC GCTTGTATCCGGAAGATGGTGTGCTGAAAG GCGACATTAAAATGGCCCTGCGCCTGAAAG ATGGCGGCCGCTATCTGGCTGACTTCAAAA CCACGTACAAAGCCAAGAAACCTGTGCAG ATGCCTGGCGCGTACAATGTGGACCGCAAA CTGGACATCACCTCTCATAATGAAGATTAT ACGGTGGTAGAGCAATATGAGCGCTCCGA GGGTCGTCATTCTACCGGTGGCATGGATGA ACTATACAAATAA

APPENDIX B

LIST OF PRIMERS

Table B 1: List of primer sequences used in this study

Name	DNA Sequence (5'-to-3')
JO1	ACCGTTTTTATTGATGGTTGTGCGCTTAAGGCTGCTCACG GTCACCTG
JO2	CACCACCACCACCACGGTGGCGGTGGATCCCAGGTGCAG CTGCAGGAAAG
JO5	GGTGGTGGCGACCATCCTCCAAAAGGATCCATGACTGAA ATCGTTGCAGATAAAAC
JO6	TCTCAGTGGTGGTGGTGGTGGTGCTCGAGTCATCAGACTT CAGGTACCTCAAAGAG
PREA24	TCTGTTCCAGGGGCCCCTGGGATCCGGTGGCGGTGGTAG CGAAAACCTGTACTTTCAGGGCGGTG
MKL2	CCGTTTTTATTGATGGTTGTGCGCTTAAGATTCATCAGCTG GGTGGCTT
pZA Ag43 atc FWD	CTTAAGCGCACAACCATCAATAAAAACGGTCG
pZA Ag43 atc REV	CACGGTGGCGGTGGATCC
JO11	CGCTGCTGCTGGTCTGCTGCTCCTCGCTGCCCAGCCGGC GATGGCCGGTGGCGGTGGATCCATG
JO12	TTCGTTTTATTTGATGCCACGCGTCTCGAGTCATTAGTGGT GGTGGTGGTGGT
PREA29	ACGCGTGGCATCAAATAAAACGAAA
PREA78	CTTTTTTTCATGGTACCCTCCTTCAGATCTTTTGAATTCTTT TCTCTATC
JO29	AAGAATTCAAAAGATCTGAAGGAGGGTACCATGAAAAAAA GAGGGGCGTT
pGB1	CTTTTTTATTATTTCCTGCAGGGCGGCCGCCCACAAGCTAACA CCACGTCGTC
pGB2	TCGAGATTTTCAGGAGCTAAGGAAGCTAAAGCATAAAACGAA AGGCCCAGTCTTTCGA

APPENDIX C

PLASMID MAPS OF CONSTRUCTS USED IN THIS THESIS

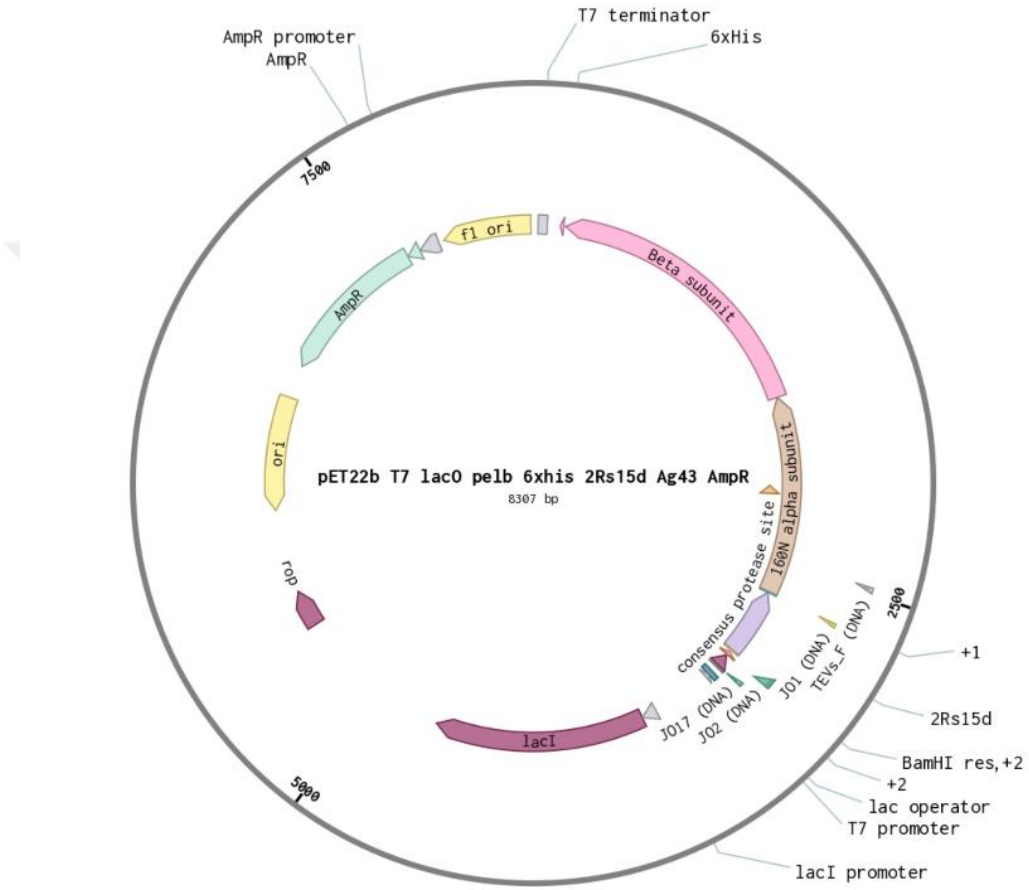

Figure C. 1: pET22b T7 lacO pelB 6xHis 2Rs15d Ag43 AmpR plasmid for surface display of nanobody.

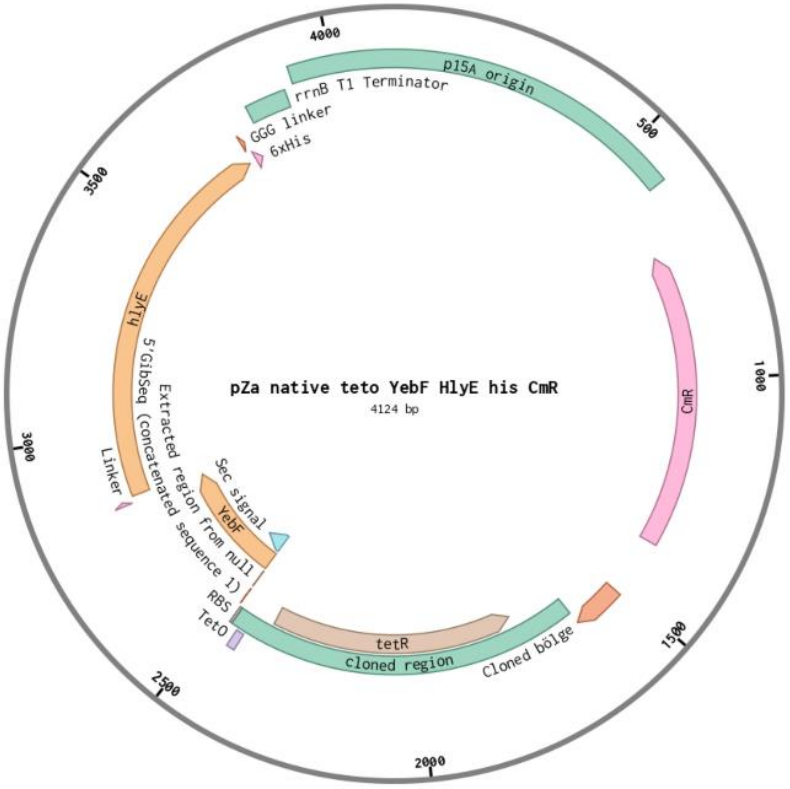

Figure C. 2: pZa native teto YebF HlyE His CmR plasmid for YebF secretion.

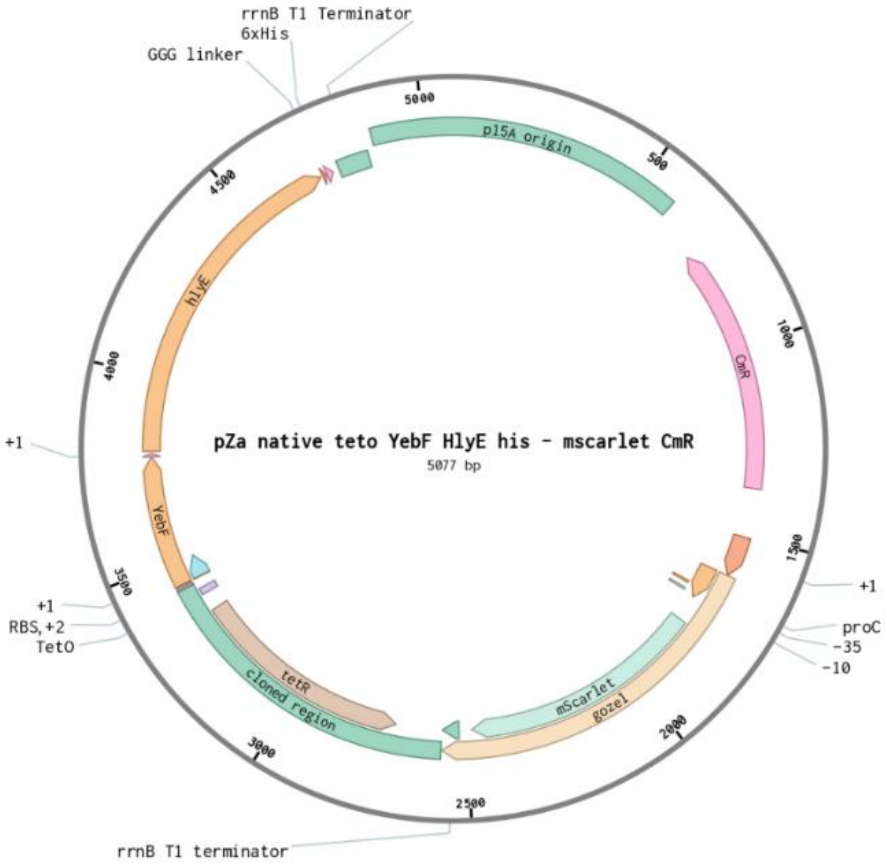

Figure C. 3: pZa native teto YebF HlyE his – mscarlet CmR plasmid for red fluorescence.

APPENDIX D

SEQUENCNG RESULTS

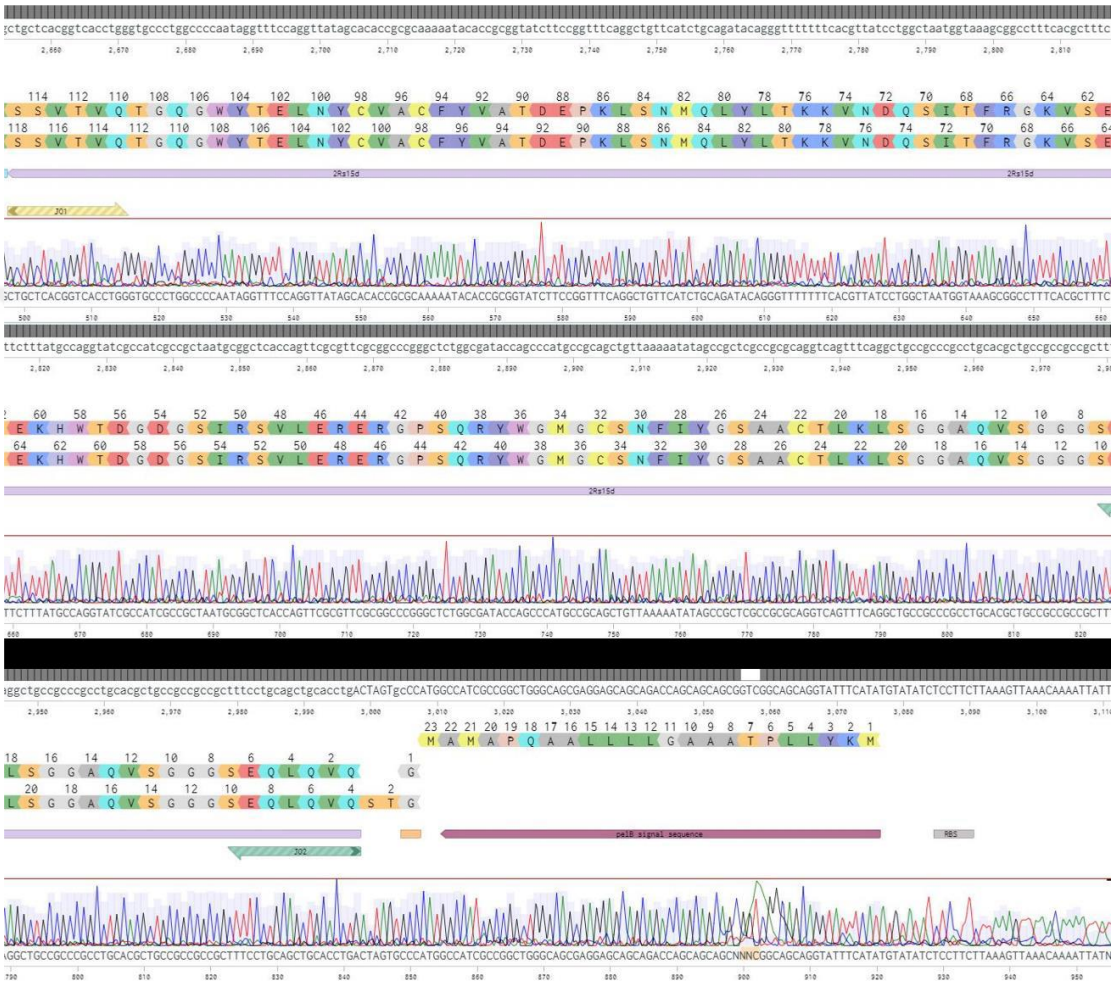

Figure D. 1: Alignment of pET22b T7-LacO pelB 2Rs15d Ag43 AmpR with sanger sequencing result via Benchling.

Figure D. 2: Alignment of pZA native pTetO HlyE Yebf 6xHis CmR sequencing result via Benchling alignment tool.

Figure D. 3: Alignment of pZA native pTetO HlyE Yebf 6xHis CmR – mScarlet using NGS sequencing.

APPENDIX E

ADDITIONAL RECIPES

Table E 1: LB Medium Recipe

Ingredients	**Amounts**
Tryptone	8 g
Sodium Chloride	8 g
Yeast Extract	4 g
Water	1000 ml

Table E 2: PCR Reaction with Q5

Ingredients	**Amounts (25 µl)**
5x Q5 Reaction Buffer	5 µl
10 mM dNTP	0.5 µl
10 µM Forward Primer	1.25 µl
10 µM Reverse Primer	1.25 µl
Template DNA	Less than 1 µg
Q5 DNA Polymerase	0.5 µl
Nuclease Free Water	Up to 25 µl

Table E 3: Double Digestion Reaction

Ingredients	**Amounts (50 µl)**
10x Cut Smart Buffer	5 µl
DNA	2 µl
Restriction Endonuclease 1	1 µl
Restriction Endonuclease 2	1 µl
Nuclease Free Water	Up to 50 µl

Table E 4: Gibson Assembly Mixture (1.3X)

Ingredients	**Amounts**
Taq Ligase	50 µl
5X Isothermal Buffer	100 µl
T5 Exonuclease	2 µl
Phusion Polymerase	6.25 µl
Nuclease Free Water	216.75 µl

Table E 5: JIMT1 Media Composition

Ingredients	**Amounts**
Low-glucose DMEM	88% (v/v)
Pen-Strep	1% (v/v)
Fetal Bovine Serum (FBS)	10% (v/v)
L-glutamine	1% (v/v)

Table E 6: MDA-MB-231 Media Composition

Ingredients	**Amounts**
High-glucose DMEM	88% (v/v)
Pen-Strep	1% (v/v)
Fetal Bovine Serum (FBS)	10% (v/v)
L-glutamine	2 mM
Non-essential amino acids (NEAA)	0.1 mM